8-2018

CHARACTERIZATION OF THERANOSTIC PEPTIDES FOR GLIOBLASTOMA MULTIFORME

Aaron Mellesmoen
aaronm949@gmail.com

CHARACTERIZATION OF THERANOSTIC PEPTIDES FOR GLIOBLASTOMA MULTIFORME

By

Aaron Mellesmoen

THESIS

Submitted to
Northern Michigan University
In partial fulfillment of the requirements
For the degree of

MASTER OF SCIENCE

Office of Graduate Education and Research

July 2018

ABSTRACT

CHARACTERIZATION OF THERANOSTIC PEPTIDES FOR GBM

By

Aaron Mellesmoen

Glioblastoma multiforme (GBM) is a type of primary CNS tumor in which viable treatment options do not exist. Standard of care including tumor resection, chemotherapy, and radiation does little to extend the 5-year survival expectancy past 5.1%. Herein, two small-peptide molecules with inherent antitumor activity, blood-brain barrier permeability, and capability for tumor-specific drug deliverance and intraoperative visualization (termed *theranostic)* were of focus. Confocal microscopy was employed to characterize *in vitro* specificity of chlorotoxin, a 4 kDa scorpion venom peptide, and rBSG, the recombinant 25 kDa non-glycosylated extracellular domain of *e*xtracellular *m*atrix *m*etalloproteinase *in*ducer (EMMPRIN; Basigin) isoform 2, toward U87 GBM and MSU 1.1 human foreskin fibroblast cell line labelling. A novel cDNA construct coding a recombinant chlorotoxin (rCTX) variant for periplasmic prokaryotic expression and histidine-tag purification was created. However, prokaryotic expression and purification of histidine-tagged rCTX was not obtainable. Confocal data also supports variable labelling activity of commercially sourced CTX and rBSG *in vitro* for both U87 and MSU1.1 cell lines. These data support further investigation of small-peptide theranostics for GBM treatment.

DEDICATION

There are many people without whom this thesis may have not been written, and whom I am greatly indebted. To my parents, who fostered my education and pursuit of my passions, and developed me into the person I am today. To Katy, my best friend and wife, who provided me with motivation and support during my failures and successes. To Robert Belton, my advisor, who respected me as if an equal and gave me the freedom to find my scientific muse. I look forward to the friendship and possible collaboration with you in the years to come. Finally, this work is dedicated to the Upper Michigan Brain Tumor Center patient's, their families, my family friend, Bob T., who succumbed to GBM, fellow graduate and undergraduate students, and professionals whom without this work would not have been made possible.

ACKNOWLEDGEMENTS

The path taken in completing this thesis has been circuitous. Its completion is attributed to the individuals who assisted, challenged, and supported me throughout the process. Following various hurdles, I am indebted to my advisor, Robert Belton, whose expertise, generous guidance, and care allowed me to develop this thesis into its final form. I am much obliged by my committee members, Dr. Amber LaCrosse and Erich Ottem, whose aid during thesis preparation and confocal microscopy, respectfully, allowed me to pursue this work. Resources for protein induction and purification provided by John Rebers is sincerely recognized. Efforts in pre-thesis brainstorming provided by Dr. John Lawrence was priceless. My peer Luke VanOsdol was critical in facilitating confocal microscopy image analysis. Undergraduates Nick Shortreed, Orry Elor, and Brandon Marshall provided project support and welcomed company in and out of lab. I am also indebted to my peer Travis Moe who provided me with lodging during my final frantic two months of data collection. Lastly, to the various members of the Upper Michigan Brain Tumor Center and NMU Biology Department who cannot go unmentioned in facilitating this work, thank you.

This thesis follows formatting guidelines provided by the Northern Michigan University Office of Graduate Education and Research. References in this thesis are written in accordance with the journal Cell: http://www.cell.com/cell/authors.

TABLE OF CONTENTS

LIST OF FIGURES

LIST OF ABBREVIATIONS

α-KG	α-ketoglutarate
5-ALA	5-amino-laevulinic acid
ABCB1	ABC-family of drug transporters
AGAR/A	LB Agar plate containing 100 μg/mL ampicillin
AGAR/A/C	LB Agar plate containing 100 μg/mL ampicillin and 25 μg/mL chloramphenicol
AKT	"A serine/threonine kinase"
AP2	Activating protein 2
BBB	Blood-brain barrier
BCA	Bicinchoninic acid analysis
BL21-rBSG	BL21-RP Codon-plus Escherichia coli (Agilent, formerly Stratagene)vharboring the pASK_IBA44 (IBA, Cat. 2-1344-000) periplasmic bacterial expression vector containing the extracellular domain of human Basigin, amino acids 23-206 of isoform 2
BrdU	bromodeoxyuridine
CBD	Collagen binding domain
CD133	Cell differentiation marker 133
CDK2	Cyclin-dependent kinase 2
CFU	Colony forming units; cells
CIC	Chloride ion channel
c-Myc	Mitogen-activated protein kinase
CSC	Cancer stem cell
D144	Delta-like ligand 4

ECM	Extracellular matrix
EGFR	endothelial growth factor receptor
EGR-2	Early growth response 2
EMMPRIN	Extracellular matrix metalloproteinase inducer
EMT	Epithelial-to-mesenchymal transition
ERK	Extracellular signal-regulated kinase
FUBP1	Far upstream element-binding partner 1
GBM	Glioblastoma multiforme
GSH	Glutathione
HA	Hyaluronan acid
HRV2	Human rhinovirus type-2
HUVEC	Human umbilical vein endothelial cell
IDH	Isocitrate dehydrogenase
IMAC	Immobilized metal affinity chromatography
JNK	c-Jun N-terminal kinase
LSB	Laemmli sample buffer
MAPK	RAS/mitogen activated protein kinase
MGMT	O6-methylguanine–DNA methyltransferase
MHC	Major histocompatibility complex
miRNA	Micro RNA
MMP-2	Matrix metalloproteinase-2
MMP-9	Matrix metalloproteinase-9
MWCO	Molecular weight cut off

MRI	Magnetic resonance imaging
mRNA	Messenger RNA
MT-MMP	Membrane-type metalloproteinase
MT1-MMP	Membrane type 1 metalloprotease
NADPH	Nicotinamide adenine dinucleotide phosphate
NOTCH1	Neurogeneic locus notch homolog protein 1 precursor
NSC	Neural stem cell
OSL	Osmotic shock lysate
PEX	Hemopexin C-terminus domain
PFA	4% Paraformaldehyde
PI3K/mTOR	Phospho-inosite-3-kinase/mammalian target of rapamycin
PMSF	Phenylmethylsulfonyl fluoride
PNET	peripheral neuroectodermal tumor
PpIX	Praporfirin-9
rBSG-2	Extracellular domain of recombinant basigin-2
rCTX	Recombinant chlorotoxin
ROS	Reactive oxygen species
RPM	Revolutions per minute
SDS-PAGE	Sodium dodecyl sulfate polyacrylamide gel electrophoresis
siRNA	Short interfering RNA
SOC	Medium containing 2% tryptone, 0.5% yeast extract, 10 mM NaCl, 2.5 mM KCl, 10 mM MgCl2, and 20 mM D-Glucose

SOC/A/C	SOC containing 100 μg/mL ampicillin and 25 μg/mL Chloramphenicol
SP1	Specificity protein 1
SVZ	Subventricular zone
TCGA	The cancer genome atlas
TERT	Telomerase reverse transcriptase
TIMP-2	Tissue inhibitor of metalloproteinase-2
TIS	Transcription initiation site
VEGF	Vascular endothelial growth factor
WCL	Whole cell lysate
WES	Whole-exome sequencing
WGS	Whole-genome sequencing
WHO	World Health Organization

INTRODUCTION

In the United States, roughly 25,000 primary malignant brain and CNS tumors are expected to be diagnosed every year. Of these tumors, 20,000 (80%) will be gliomas (of astrocytic origin) ranging from World Health Organization (WHO) grades I-IV. An increase in tumor grade correlates with a poor prognosis. Grade IV astrocytic gliomas, also known as glioblastoma (GBM), will account for approximately 12,000 of these cases (or 55.1% of gliomas). Although the incidence of GBM is low in comparison to all other tumor types, its 5-year survival rate is only 5.1% (Ostrom et al., 2015). Therefore, further research into this disease is warranted.

GBM Bioinformatics

Conventionally, gliomas have been qualitatively graded and diagnosed microscopically by morphological criteria of the resected tumor sample. Cell characteristics such as size, shape, pleomorphism (i.e. mitotic figures), vascularity, and tissue necrosis positively correlate to GBM presence (Zhang et al., 2000). Because GBMs and other glioma tumors are composed of a heterogeneous cell population, the tumor-grading system based on this qualitative and subjective diagnostic approach needed to be altered. In the 1990s, immunohistochemical methods using antibodies to probe for specific epitopes of varying glioma grades were introduced (Reviewed by Zhang et al., 2000). An example of such epitope for highly proliferating cells is nuclear protein ‘ki-67’ (Scholzen and Gerdes, 2000). As a facilitator of ribosomal RNA synthesis (Rahmanzadeh et al., 2007), ki-67 protein is only expressed during active stages of the cell cycle

(Bruno and Darzynkiewicz, 1992) with increasing expression during S phase (Darzynkiewicz et al., 2015). Other markers of interest included cyclin (or proliferating-cell nuclear antigen), an effector protein which increases DNA polymerase VI activity (Bauer and Burgers, 1988). Cyclin-dependent kinase 2 (CDK2) expression is elevated in GBM when compared to normal brain, is functionally-required for tumor proliferation, and is facilitative of evading radiation-induced apoptosis (Wang et al., 2016). Additionally, a synthetic nucleoside analog of thymidine, bromodeoxyuridine (BrdU), was visualized after its incorporation into the DNA of rapidly-dividing cells during the S-phase of the cell cycle (Hoshino et al., 1985). However, as reviewed by Zhang et al., determining the grade of a heterogenous glioma tumor by identifying only a few tissue epitopes and morphologies does not reveal the full "signature" of the tumor (2000). Therefore, a quantifiable cDNA microarray or genetic profiling regime was needed. In 2003, Nutt et al. used microarray technology to probe for ~12,000 genes in roughly 100 gliomas and found that molecular classification of gliomas correlated better with clinical outcomes than standard pathology.

Further meta-data type studies involving bioinformatics methods, clinical data, and varying "-omics" data were performed. In 2010, Verhaack et al. successfully used bioinformatics methods to categorize 206 GBM patients' samples into four different molecular subtypes based on mutational data in 601 genes and full-DNA sequences data. Of these four molecular subtypes (classical, mesenchymal, proneural, and neural), it was found that chemotherapy and radiation co-treatment was effective in prolonging patient survival in all but the proneural subtype (Verhaack et al., 2010). Thus, it was suggested

that only using MGMT (O6-methylguanine–DNA methyltransferase) promoter methylation status for determining temozolomide use in all GBMs may not be suitable (as described later).

In 2015, whole-exome sequence[1], DNA copy number, DNA methylation status, mRNA and miRNA expression levels, and protein expression data from 293 primary low-grade (II-III) adult gliomas were correlated with clinical outcome data via unsupervised clustering[2] by The Cancer Genome Atlas research network (TCGA). Histological grade was not adequate in predicting patient outcome (i.e. indolent to GBM progression). Bioinformatics methods revealed three prognostically-significant molecular subtypes of low-grade gliomas delineated by isocitrate dehydrogenase (IDH) mutation status, 1p/19q chromosome arms co-deletion presence, and TP53 status (TCGA, 2015). Although some of these markers were previously correlated with tumor growth, their concordance with a clinical outcome was unknown. Patients harboring (the mutually exclusive enzyme-activity decreasing (Yan et al., 2009)) mutations within metabolic IDH isozymes 1 or 2[3] and 1p/19q co-deletion also had mutations in CIC (a membrane chloride ion channel), FUBP1 (far upstream element-binding partner 1; a ssDNA binding protein

1 Whole-exome sequencing (WES) is a cheaper alternative to whole-genome sequencing (WGS). WES provides targeted sequencing of all protein-coding genomic regions (i.e. the exome) which collectively account for 1% of the genome and 85% of disease-associated variants (van Dijk et al., 2014).

2 Unsupervised clustering is the compiling of data into groups without pre-specified group or data labels.

3 IDH1 and 2 are localized to the cytosol and mitochondria, respectively, and function to produce Kreb cycle-independent nicotinamide adenine dinucleotide phosphate (NADPH) from NADP+ via catalyzing the isocitrate to α-ketoglutarate (α-KG) (Pollard and Ratcliffe, 2009). Although mutually exclusive, mutations within either of these isozymes (with greater prevalence of that in IDH1; Yan et al., 2009) occur within the enzyme's catalytic domain responsible for isocitrate binding (Xu et al., 2004). Over 85% of glioma IDH1 mutations occur via a heterozygous missense mutation of arginine to histidine at amino acid 132 (i.e. R132H; Watanabe et al., 2009). With IDH2, the same mutation occurs at amino acid 172 (Yan et al., 2009). The consequence is a decrease in NADPH, a cofactor necessary for maintenance of glutathione (GSH)

responsible for initiating downstream c-Myc, a constitutively active onco-transcription factor), NOTCH1 (neurogeneic locus notch homolog protein 1 precursor; a transmembrane protein involved in stem cell maintenance as reviewed by Stockhausen et al. (2010)), and TERT's promoter (telomerase reverse transcriptase; which is responsible for telomerase-length maintenance (Killela et al., 2013)). These findings aligned with a better clinical patient outcome (TCGA, 2015). Lastly, low-grade tumors with no IDH mutation had similar clinical outcomes reflective of GBM (TCGA, 2015).

These studies were suggestive of gliomas arising and progressing to higher grades due to multiple gliomagenesis mechanisms (Verhaack et al, 2010; TCGA, 2015). This assumption was supported by independent work analyzing 1p/19q chromosomal co-arm deletion, and IDH and TERT promoter mutation status, in 1087 gliomas of varying grades (Eckel-Passow et al., 2015). Results revealed five groups of gliomas based on these three markers alone, and that multiple distinct mechanism of gliomagenesis could be occurring (Eckel-Passow et al., 2015).

GBM Biology

These findings do not support the "stochastic" model of cancer progression which states that all cells of a tumor are similar in their carcinogenic capability, and that any one of them could metastasize to initiate another tumor. If somatic cells need between 4-7

levels required to neutralize reactive oxygen species (ROS) (Yan et al., 2009). Glioma benefit from IDH mutation due to its role in facilitating genome-wide epigenetic changes (Reviewed by Yan et al., 2009) and cellular accumulation of HIF-1α, a transcription factor specific for angiogenesis, metabolism, growth and differentiation, apoptosis, autophagy, and cell motility pathways (Fu et al., 2012).

independent mutations to become cancerous (Hanahan & Weinberg, 2000), it is assumed that further mutation metastatic sites may propagate tumor formation. However, recent bioinformatics data, as discussed above, supports a "hierarchical" model in which only a subset of the tumor cell population can self-renew, propagate, and differentiate into other cell types constituting the tumor mass (Visvader and Lindeman, 2008). Taken together, it is implied that cancer stem-cells (CSCs) may be the root cause of gliomagnesis and GBM formation.

To test this hypothesis, Zheng et al. used a conditional murine tumor suppressor gene knockout model containing a homozygous loss of p53 and heterozygous loss of PTEN and found that 73% (N=57) of the colony passed away after 28 weeks due to neurological symptoms (2008). Upon autopsy, all deceased mice had grade III and IV (GBM) gliomas with similar pathology to that observed in human primary GBM (i.e. cell pleomorphism, diffuse infiltrative borders, necrosis, and pseudopalisading and microvascular proliferation) (Zheng et al., 2008). Subsequent *in vitro* work with neural stem-cells (NSCs) harboring double-null inactivated p53 and PTEN resulted in promoted c-Myc expression which facilitated NSC-enhanced self-renewal capacity and impaired differentiation. Follow-up work by Wang et al. corroborated these findings by demonstrating that *in vitro* treatment of CSCs with short interfering RNA (siRNA) knockdown of c-Myc reduced cell proliferation and increased apoptosis, as compared to differentiated cells, which were unaffected by the c-Myc siRNA (2008). Based on these works, NSC DNA modification may be one step in developing a CSC to which gliomagenesis is the result. However, it should also be noted that necrosis and

microvascularization are two characteristics of a "developed" GBM which facilitate GBM CSC maintenance (Reviewed by Persano et al., 2013). Therefore, cellular environment may also have a role in influencing gliomagenesis (Reviewed by Persano et al., 2013).

NSC interact with their cellular environment to become differentiated cell types needed for neural function. For example, in mice it is known that NSCs within the "perivascular niche" of the SVZ (subventricular zone) migrate to the olfactory bulb (Vescovi et al., 2006). These migrating cells express both stem (i.e. Nestin+) and differentiated (i.e. GFAP+) cell markers which can also be indicative of neurons and glia, respectfully (Vescovi et al., 2006). Furthermore, the proliferation, renewal, and differentiation of NSCs within the SVZ are influenced by the juxtacrine and paracrine interactions with nearby epidermal (Gonzalez-Perez and Alvarez-Buylla, 2011) and immune (Gonzalez-Perez et al., 2010) cells, extracellular matrix, microglia, vasculature, neurons, and cerebral spinal fluid (Reviewed by Ihrie and Álvarez-Buylla, 2011). There are various factors which influence a NSC's activity and these same factors may also influence a NSCs transformation into and maintenance as a CSC. For example, vascular endothelial cells can facilitate self-renewal and proliferation of undifferentiated (i.e. CD133+, cell differentiation marker 133) CSCs (Calabrese et al., 2007) via a juxtacrine Notch-ligand expression D114 (Delta-like ligand 4) mechanism (Zhu et al., 2011). Notch is one cell-membrane protein responsible for stemness and self-renewal of GBM CSCs (Zhu et al., 2011). However, this process of CSC to non-functional vascular (endothelial cell) interaction occurs near hypoxic (low-oxygen) regions of the tumor (Vaupel et al.,

2004). Near the necrotic core of the GBM tumor mass, oxygen levels decrease (i.e. 2.5% - 0.1% O_2 saturation) (Evans et al., 2004), Hypoxia Inducible Factor 1-α activity increases (HIF-1 α; a transcription factor), extracellular pH decreases, and an increase in resistance to chemotherapy and radiation occurs (Vaupel et al., 2004). The HIF family of transcription factors are deubiquitinated and/or expressed under low O_2 conditions. A consequence is the expression of various glucose transporters, angiogenic and hematopoietic growth factors, and mitogens (Reviewed by Persano et al., 2013). Also, low oxygen levels impeded photon-radiation treatment (if not performed at 3x the normal dose) as DNA damage via oxygen free radicals decreases due to the lack of oxygen to interact with intracellular water after its photon-mediated excitation (Spence et al., 2008).

In summary, independent mutation mechanisms within NSC or other cell types may lead to CSC formation whose inherently aberrant self-renewal and differentiation pathways may give rise to a fast-growing heterogeneous cell population. CSC activity is likely supported by the local cell environment which includes the supporting non-functional vasculature of endothelia, termed the "perivascular niche", that is responsible for secreting various cell factors to maintain CSC "stemness" (Calabrese et al., 2007). As the glioma progresses to a GBM, necrotic conditions develop which promote therapeutic insensitivity and CSC perpetuation. Therefore, the current clinical regimen in treating GBMs may need to be addressed and altered in accordance to these findings.

Standard & Investigated GBM Treatments

Current tumor treatment includes imaging, surgery, chemotherapy, and radiation. Innovative therapies are under development, but patient outcomes are still marginal due to the failure of our current efforts to address the various aspects of GBM biology, as discussed above. As of now, patients with brain tumor symptoms undergo non-invasive magnetic resonance imaging (MRI) to determine the location and size of the tumor. Although gliomas are highly-invasive, they are usually confined to the cranium (Stupp et al., 2014). As such, MRI of the spine is not usually performed. Next, perioperative medications can be given to patients before and after tumor resection to decrease the effect of tumor and surgical-associated edema. Typically, the corticosteroid dexamethasone is given at a dose of 8-16 mg per day (Stupp et al., 2014). Additionally, anti-seizure medications may be implemented if the patient has a history of seizures, or possibility of postoperative seizures. Historically, first generation antiepileptic medications such as phenytoin have been administered. However, their complications with chemotherapeutics (excluding temozolomide) has led to the prescription of similar but alternative therapeutics such as levetiracetam and valproic acid (Stupp et al., 2014).

During surgical removal of GBM, maximum removal of the bulk tumor and its diffuse tumor margins is conducted while respecting surrounding neural tissue so neurological function may be preserved. Although more common in Europe than in the United States, fluorescence-guided resection via administered 5-amino-laevulinic acid (5-ALA) may also be employed (Stummer et al., 2006). 5-ALA is internalized by GBM cells and is converted to its fluorescent metabolite Protoporphyrin IX (PpIX) via the

heme pathway (Rick et al., 1997). As it stands, it is difficult to discriminate tumor and its margins from healthy brain tissue. Tumor-specific fluorescence enables the surgeon to grossly delineate healthy and diseased tissues to optimize surgery. If total resection is not possible, a biopsy is taken. A pathological and molecular analysis (i.e. LOH 1p/19q, MGMT promoter methylation, etc.) is then performed for diagnosis and downstream patient treatment design (Stupp et al., 2007).

Following surgical removal or biopsy of the tumor, molecular analysis is performed to obtain the methylation status of the MGMT (O6-methylguanine–DNA methyltransferase) gene promoter since it is clinically significant and beneficial (Esteller et al., 2000). The promoter element of the MGMT gene, located on chromosome 10q26, can be endogenously methylated to inhibit its expression as a DNA-repair protein. MGMT functions by removing alkyl groups from the O6-position of guanine bases (Hegi et al., 2005) which may otherwise lead to cytotoxicity and apoptosis (Ochs and Kaina, 2000). Temozolomide is one such cytotoxic prodrug which modifies DNA purine bases (i.e. an alkylating agent) via the addition of a methyl group adduct to futilely induce DNA mismatch repair, DNA stand breaks with replication fork collapse, and ultimately apoptosis (Reviewed by Zhang et al., 2012). Thus, normal expression of MGMT in GBM (which is allowed by a non-methylated MGMT promoter) reduces the effectiveness of standard chemotherapy regimens involving alkylating agents such as temozolomide (Silber et al., 1999; Hegi et al., 2005). Temozolomide is a standard chemotherapeutic for GBM which when combined with radiation over multiple treatment cycles, as supposed to radiation alone, has been shown to improve the 5-year overall patient survival from

~2% to ~10% (Stupp et al., 2009). However, if the patient does survive, they are likely to suffer from cognitive disabilities caused by the radiation and adjuvant chemotherapy.

Patients diagnosed with frontal or temporal lobe tumors commonly display decreased cognition following treatment. Tumor location, chemotherapy, and radiation regimes are contributing factors in amplifying long-term cognition deficits. For example, due to the nonspecific nature of radiation, roughly 50-90% of brain tumor survivors present with spatial memory, attention, or problem-solving deficits (Reviewed by Sacks-Zimmerman et al., 2015). Necrotic cell death due to neuron demyelination and microvascular injury is induced which can lead to decreased white-matter tract density and cognitive deficits (Reviewed by Sacks-Zimmerman et al., 2015). Still, many patients enter remission as the standard therapy is not effective for all patients. Therefore, other experimental tumor-specific treatments which rely on 'tumor biology' for efficacy and selectivity are being explored.

Antiangiogenic treatments are being investigated for patients who enter remission or find temozolomide ineffective (Wen and Kesari, 2008). These treatments are an attempt to disrupt the "perivascular niche", a network of non-functional vascular endothelial cells which maintain CSC "stemness" during gliomagenesis (Calabrese et al., 2007). Following a phase I demonstration of minimal toxicity in recurrent GBM patients, a phase II clinical trial investigating the efficacy and safety of Cilengitide, an angiogenesis blocker molecule, for recurrent GBM monotherapy proved to be efficacious with a 15% progression-free survival rate of 6 months (study primary end-point) and

median overall survival (study secondary end-point) of 10 months observed (Reardon et al., 2008). Cilengitide interrupts angiogenesis (and induces apoptosis) by inhibiting the FAK/src/AKT pathway (Oliveira-Ferrer et al., 2008) through competitive binding to the $\alpha v\beta_3$ and $\alpha v\beta_5$ integrin adhesion receptor amino acid sequence Arg-Gly-Asp (i.e "RGD") (Goodman et al., 2002). GBM overexpress such integrins which makes them a "bulls-eye" for targeted therapy (Oliveira-Ferrer et al., 2008). Briefly, integrins are transmembrane proteins which adhere the cell to the extracellular matrix to influence cytoskeletal arrangement, cell cycle regulation, and trafficking of membrane-bound receptors to the cell surface (Giancotti & Ruoslahti, 1999). Additionally, the monoclonal anti-VEGF antibody Bevacizumab (Avastin) is another antiangiogenic therapy which, as a monotherapy for recurrent GBM, has demonstrated a 6-month survival rate of ~43% and median overall survival rate of ~9 months (Friedman et al., 2009). Although functional, antiangiogenic treatments are still ineffective in extending the "hallmark" median overall survival for GBM patients of 12 to 15 months (Wen and Kesari, 2008). However, oncolytic viral therapy is another experimental GBM treatment being investigated.

The concept of using attenuated oncolytic virotherapy was first introduced in 1991 (Martuza et al., 1991). Since then, 15 viruses have been investigated, with several advancing to clinical trials (Reviewed by Wollmann et al., 2012). The most promising of these used an engineered poliovirus to target GBM cells following delivery via intracranial catheter inserted after tumor biopsy. The wild-type poliovirus is a positive-stranded (mRNA-like) RNA virus which induces neurotoxicity in motor neurons.

Toxicity is first mediated by the expression of its receptor Necl-5 (CD155) on the cell surface (Wollmann et al., 2012). Physiologically, Necl-5 is a homophilic transmembrane glycoprotein which forms adherens junctions to influence intercellular interactions, cellular shape, and adhesion of the cell's actin cytoskeleton to their lateral membrane (Reviewed by Meng and Takeichi, 2009). However, Necl-5 is over-expressed on GBM, which makes it an exploitable marker for treatment (Merrill et al., 2004). Once the wild-type poliovirus is internalized by the host cell, its internal ribosomal entry site (IRES) sequence within its RNA genome binds to free eIF4E (cap-binding translation factor) protein to recruit 40S and 60S ribosomal subunits for transcription and subsequent viral replication and lysis of the host cell (Wollmann et al., 2012). However, because viral infection of the wild-type (and GBM therapeutic) polioviruses cannot delineate between GBM and all other cells which express Necl-5 to some degree, the IRES sequence was removed and replaced for a null variant from the human rhinovirus type-2 (HRV2) virion (Goetz and Gromeier, 2010). Thus, therapy efficacy would not be due to the cell surface expression of Necl-5 by GBM or healthy cells, but instead be due to the uniquely aberrant intracellular signaling cascades within GBM cells.

One hallmark of GBM cells is the upregulation of signaling pathways such as the phospho-inosite-3-kinase/mammalian target of rapamycin (PI3K/mTOR) and RAS/mitogen activated protein kinase (MAPK) leads to increased phosphorylation of eIF4E, which in addition to the inherent self-amplification and high-mutation rate of RNA virions, may lead to 5'-cap-independent translation of virions within the host GBM cell (Goetz and Gromeier, 2010). Thus, this recombinant poliovirus only functions within

GBM cells. With these findings, a phase 1 clinical trial has been completed but a published report discussing its conclusions is yet to be released at the time of this writing (Bigner, 2011).

Until now, most attempts to treat GBM, a highly-heterogeneous and diffuse brain tumor, have been stymied by various factors. First, the brain is protected by a blood-brain barrier (BBB) which inhibits most systemic and non-invasive chemotherapies from reaching the brain (Bruce et al., 2015). Furthermore, the brain is a terminally-differentiated organ with limited ability to regenerate following global insult, and thus ablative chemotherapy and radiation are not practical (Bruce et al., 2015). Also, radical resection is not always attainable due to possible loss of neural regions responsible for cognitive processes and motor activities. Even so, bioinformatics studies support that therapeutic-resistant CSCs, through different genotype modalities, may give rise to molecularly-distinct GBMs; thus, different therapies may have confounding efficacies between different GBM cases. Therefore, to gain leverage in treating GBMs which have an array of tumor-driving molecular signatures, the initial source of the cancer (i.e. CSCs) must be targeted while also addressing the phenotypic pillars in which all GBMs depend on.

Utilizing GBM's Pillars of Disease Progression

Phenotypically, GBM are heterogenous in cell type and express an increased ability to proliferate, oncomodulate (i.e. alter the tumor surroundings), and metastasize to sites away from the tumor bed. These facets of GBM biology are major contributing

factors to GBM lethality (Wojton et al., 2015). GBM's lethality may be due to a subpopulation of CSCs which reside not only within the perivascular niche, but also within the tumor's necrotic core. Coincidentally, CSCs have a high-level of chemotherapy and radiation therapy resistance and are distinguishable via CD133 cell-marker expression (Kalkan, 2015). CD133 (or Prominin-1) is a transmembrane glycoprotein expressed on hematopoietic stem cells (Horn et al., 1999), endothelial progenitor cells (Corbeil et al., 2000), and in other physiologically normal cell types distributed throughout the body (Mizrak et al., 2008; Shmelkov et al., 2005). CD133 expression has also been used as a target in isolating cell subpopulations from primary brain tumors which were observed to be highly prolific, self-renewable, and differentiable. These cells *in vitro* had the capacity to differentiate and produce cells which exhibited cell morphologies from the initial patient brain tumor (Singh et al., 2003).

CD133 expression levels on GBM CSCs has been studied to be recognized by a seven amino acid peptide motif (i.e. TR peptide) conjugated to a DSPE-PEG micelle carrying coumarin-6 (Wang & Zhang, 2015), a naturally-occurring plant compound with anticancer activity (Reviewed by Emami & Dadashpour, 2015). However, CD133 is also still expressed by cells of non-neoplastic nature, and therefore CD133-mediated CSC targeting may have significant off-target effects. A tumor-specific targeting molecule is required and research demonstrates that targeting differentiated cancer cell types with short peptides is possible.

Use of Chlorotoxin in GBM

Chlorotoxin is a 36 amino acid (4 kDa) short-chain disulfide containing neurotoxin derived from the venom of the deathstalker scorpion (*Leiurus quinquestriatus*) that induces rigid paralysis in arthropods and crayfish by binding to chloride ion-channels in a dose-dependent manner (DeBin et al., 1993). Chlorotoxin's efficacy is due to its unique protein structure. Its secondary structure is comprised of one α-helix (amino acids 11 to 21), three β-sheets (amino acids 1 to 4, 26 to 29, and 32 to 36), and eight disulfide bonds between Cys5-Cys28, Cys16-Cys33 and Cys20-Cys35, and Cys2-Cys19 which links the N-terminus with the last segment of the α-helix (Lippens et al., 1995). Over a range of pH values, (i.e. 2.8 and 5.5), chlorotoxin maintains its (cysteine-mediated) stability, basicity, and positive-charge (Reviewed by Ojeda et al., 2016).

The stability, chlorine-ion channel affinity, and therapeutic activity of chlorotoxin may be attributed to two semi-distinct disulfide bond structural motifs. Chlorotoxin has the common short-chain scorpion toxin motif 'cysteine-stabilized α-helix-β-sheet fold (CSα/β) (Bontems et al., 1991) represented by bonds (CysII-CysVI, CysIII-CysVII and CysV-CysVIII) (i.e. Cys5-Cys28, Cys16-Cys33 and Cys20-Cys35) (Reviewed by Ojeda et al., 2016). The inhibitor cysteine knot (IKC) motif is characterized by chlorotoxin's disulfide bonds Cys2-Cys19, Cys5-Cys28 and Cys16-Cys33 (i.e. CysI-CysIV, CysII-CysVIand CysIII-CysVII) (Reviewed by Ojeda et al., 2016) which has been implemented in drug-design due to its chemical, biological, degradative, thermal, and pH stability (Craik et al., 2001). Due to chlorotoxin's amino acid length and homology to other

potassium channel blocker proteins, it is part of the alpha subfamily of the CSα/β motif-containing protein group (Kuzmenkov et al., 2015).

α-CSα/β motif-containing proteins are known to bind to voltage-gated potassium (or other) ion channels at nanomolar concentrations by either the affinity of β-hairpin residues to the channel pore (Yu et al., 2010) or by forming a "functional dyad" comprised by a lysine side-chain entering the channel pore with involvement of another tyrosine, phenylalanine, or leucine residue (Banerjee et al., 2013). In addition, a salt-bridge between the negatively-charged ion-channel and positively-charged protein amino acids may also be of influence (Lipkind and Fozzard, 1997; Review by Kuzmenkov et al., 2016). Thus, chlorotxin's affinity and inhibition of chloride-ion channels is hypothesized to be due to physical blockage of the channel pore. Coincidentally, this same mechanism and characteristics effective for chlorotoxin's natural function may be therapeutically advantageous.

In 1995, chlorotoxin was first applied to human primary brain tumor and astrocytoma cell lines *in vitro* which demonstrated via whole-cell patch-clamp recording that chlorotoxin inhibits chloride-ion channel function (Ullrich et al., 1995). Three years later, the first *in situ* study of chlorotoxin and glioma cells was conducted which found that chlorotoxin labeled with radioactive iodine (i.e. 125I and 131I) was able to selectively bind and localize to glioma cells without accumulating in normal brain, kidneys, or colon cells (Soroceanu et al., 1998). Transwell migration assay further showed that a 5 μM concentration of chlorotoxin was able to bind to glioma chloride-ion

channels and alter cell shape and volume which ultimately inhibited cell migration (Soroceanu et al., 1999). However, because GBMs were believed to be derived from glial cells, the neural support cells of neuroectodermal origin, it was unknown if chlorotoxin would non-specifically bind to all cells of neuroectodermal origin (i.e. peripheral nervous system neurons, Schwann cells, connective tissue of face and neck, endocrine cell, etc.) (Lyons et al., 2002). Histochemical staining of varying frozen and paraffin-preserved neuroectodermal tumor tissue sections showed that synthetic and native biotin-labeled chlorotoxin was able to delineate gliomas, peripheral neuroectodermal tumors (PNETs), medulloblastomas, neuroblastomas, ganglioneuromas, melanomas, primitive PNET, adrenal pheochromocytomas, small cell lung carcinoma, and Ewing's sarcoma without binding to brain (which including normal, Alzheimer's, and Parkinson/schizophrenic samples), skin, kidney, and lung samples from the same specimen (Lyons et al., 2002).

Later, Deshane et al. identified a second target of chlorotoxin on glioma cells called matrix metalloproteinase-2 (MMP-2), in complex with $\alpha v\beta_3$ integrin, MT1-MMP (membrane type 1 metalloprotease), and tissue inhibitor of metalloproteinase (TIMP)-2 (2002). Gelatinases such as MMP-2 and MMP-9 are ectopically expressed as inactive zymogens of 72 and 92 kDa, respectively, and work to degrade the extracellular matrix (ECM) for cellular remodeling and retrieval of ECM-harbored mitogens needed for cellular growth (Reviewed by Bauvois, 2012). Although overexpressed on glioma cells, ectopic MMP-2 presence decreases with chlorotoxin binding; MMP-2 is not expressed in normal brain cells (J. Deshane, C.C. Garner, & H. Sontheimer, 2002). MMP-2's structure is composed of a hydrophobic signal-secretion domain, a propeptide domain which is

cleaved to reveal active MMP, an enzymatic domain which has a zinc-binding site and collagen binding domain (CBD) (Reviewed by Björklund & Koivunen, 2005), and a hemopexin C-terminal domain (PEX) adjacent to the catalytic domain via a flexible hinge (Reviewed by Bauvois, 2012). TIMPs by themselves can mediate cell survival, migration, survival, and angiogenesis, but they (i.e. TIMP-2) also bind the MMP PEX domain (Reviewed by Bauvois, 2012).

On the cell surface, latent MMP-2 can become activated when its PEX domain complexes with TIMP-2 and membrane-type matrix metalloproteinase-1 (MT1-MMP; via its catalytic domain; Reviewed by Bauvois, 2012). Once activated, MMP-2 has been shown to interact with integrin $\alpha v\beta_3$ via its PEX domain (Rupp et al., 2008). In A549 lung cancer cells, *in vitro* siRNA knockdown of MMP-2 reduces phosphatidylinositol 3-kinase and AKT phosphorylation (signaling pathways) leading to decreased HIF-1α expression and vascular endothelial growth factor (VEGF) presence to inhibit vascular sprouting, endothelial cell differentiation, and microtubule formation (i.e. angiogenesis) (Chetty et al., 2010). In similar studies, VEGF expression was also decreased by molecular inhibition of MMP-2 (via ARP-100) via the integrin $\alpha v\beta_3$-mediated PI3K/AKT signaling pathway (Chetty et al., 2010).

Finally, endocardial epithelial cells from developing quail hearts, when expressing MMP-2 and $\alpha v\beta_3$ *in vitro*, can undergo an epithelial-to-mesenchymal transition (EMT) which facilitates its invasion into a collagen gel (Rupp et al., 2008). Internalization of chlorotoxin, via its binding to the MMP-2 complex, may be mediated

via co-internalization of ectopic MT1-MMP. Jiang et al. demonstrated that MT1-MMP is internalized via a clathrin-coated vesicle to early endosomes via a dynamin-dependent process (2001). Cell surface MT1-MMP is maintained by clathrin-dependent endocytosis, and TIMP-2 stabilizes MT1-MMP surface presence (Hernandez-Barrantes et al., 2000); this process optimally occurs at 37 °C (El-Ghlban et al., 2014). These results indicate chlorotoxin's affinity for cells expressing an angiogenic and invasive phenotype mediated by MMP-2 complex, and that chlorotoxin may be internalized by glioma cells via clathrin-coated pits.

Chlorotoxin has also been shown to interact with annexin-2 (Kesavan et al., 2010). Synthetic chlorotoxin (TM601) was able to bind ectopic annexin-2 of U373-MG glioma and human umbilical vein endothelial cell (HUVEC) cell lines which inhibited angiogenesis and transwell migration *in vitro* (Kesavan et al., 2010). In general, annexins are a pleiotropic class of proteins which are composed of a highly-conserved 310 amino acid C-terminus "core" of four "annexin repeats" (of which each has 5 alpha helices) and an N-terminus "head" which is unique to every annexin (Gerke and Moss, 2002). The extracellular C-terminus also contains type-2 Ca^{2+} binding sites which facilitate interaction with phospholipids of the plasma membrane while the intracellular N-terminus binds to cytoplasmic proteins (Gerke and Moss, 2002). However, annexin-2 is ectopically overexpressed on GBM cells (Wang et al., 2014) which may be explained by its ulterior function in facilitating cholesterol-rich lipid raft formation via its interaction with CD44, a cell-surface receptor for hyaluronic acid (HA) (Oliferenko et al., 1999). In the presence of radiation, annexin-2 inhibits apoptosis by mediating the nuclear

translocation of Nf-kβ to prevent DNA damage (Waters et al., 2013). Annexin-2 knockdown via siRNA in cancer cells increases reactive oxygen species (ROS) levels which leads to p38MAPK (mitogen-activated protein kinase)/c-Jun N-terminal kinase (JNK)/AKT mediated apoptosis (Madureira et al., 2011). Also, *in vivo* siRNA-mediated knockdown of annexin-2 in the mouse GBM (GL261) cell line halts tumor growth and inhibits cell migration in U87MG GBM cells (Zhai et al., 2011).

Together, annexin-2 and CD44 co-localized into lipid rafts and not into caveolin-coated pits of EpH4 immortalized mouse mammary epithelial cell line (Oliferenko et al., 1999). Lipid rafts are organized regions of the cell membrane which facilitate signal transduction events and cytoskeletal interactions on the plasma membrane (Oliferenko et al., 1999). Conveniently, lipid rafts and various cell-membrane proteins located therein mediate many of the functions needed for cancer maintenance and progression. One example of such a protein is basigin, an evolutionary-conserved protein with pathological and physiological pleiotropic function.

Basigin, a Pleiotropic Transmembrane Protein

Basigin was independently characterized in the early 1990s by multiple investigators. Basigin was first functionally characterized using a human lung carcinoma and fibroblast co-culture system. Expressed on the surface of carcinoma cells and released into the conditioned media presumably through microvesicle shedding, basigin induced expression of collagenase by fibroblasts (Biswas, 1984). Cloned from F9 embryonal carcinoma and recognized as novel single-chain type I transmembrane

glycoprotein in the immunoglobulin (Ig)-like superfamily of proteins, it's homology to the β-chain of major compatibility complex (MHC) class-II antigen and IgV domain and similarity in amino acids length between the disulfide bridges between IgV and C-like globulins suggest an evolutionary-conserved role. In addition, the same study reported of basigin mRNA presence in embryonic carcinoma cells *in vitro*, within mouse embryos, and in various adult mouse tissues (Miyauchi et al., 1990). Then-termed tumor cell-derived collagenase-stimulatory factor (TCSF), Basigin was later named EMMPRIN (EXtracellular Matrix Metalloproteinase INducer) due to its ability to stimulate secretion of MMP-2 and -3 by fibroblasts (Biswas et al., 1995). Further work confirmed basigin's pleiotropic role through its study in neuronal-glia patterning of the developing retina (Fadool & Linser, 1993), fertility, learning, memory, sensory perception (Ochrietor & Linser, 2004), and neuroinflammation (Agrawal & Yong, 2011).

Expression of the human basigin gene (*BSG*) is represented through four differentially-spliced and promoted isoforms entitled basigin-1, -2, -3, and -4 (Liao et al., 2011) *BSG* is comprised of 10 exons and located on chromosome 19p13.3 (Kaname et al., 1993). Isoforms 1 and 2 are expressed through a transcription initiation site (TIS) located ~1,500 b.p. upstream of exon 2 which contains a CpG island-rich promoter region containing a TATA box, suppressor elements, and notably multiple enhancer sequences specific for specificity protein 1 (Sp1), activating protein 2 (AP2), and early growth factor 2 (EGR-2) transcription factor families (Guo et al., 1998; Liang et al., 2002). Basigin-2 is the most studied and ubiquitously-expressed isoforms which is characterized by having two (Ig)-like extracellular domains; basigin-1 includes an extra (Ig)-like

domain due to the addition of translated exon 3 (Hanna et al., 2003). Basigin-3 and -4 utilize an alternative promoter region located 1,227 nucleotides upstream of basigin-2's TIS (Liao et al., 2011). Translation of basigin-3 begins at the start codon preceding exon 5 to produce a peptide containing only one extracellular (Ig)-like domain (Belton et al., 2008). Basigin-4 mRNA does not include exon 4 and thus results in a peptide with only one (Ig)-like domain followed by an extra 11 amino acid N-terminal signal sequence encoded by exon 1 (Liao et al., 2011). Interestingly, the isoforms' cytoplasmic and transmembrane domains are conserved with respect to amino acid sequence (aside for basigin-4) and number (Belton et al., 2008). The 41 residue cytoplasmic domain contains two phosphoserines (Weidle et al., 2010) and is functional in interacting with caveolin-1 (a negative regulator of basigin self-association, glycosylation, and MMP induction; Tang et al., 2004), integrins $\alpha_3\beta_1$ and $\alpha_6\beta_1$ (Dai et al., 2009; Li et al., 2012), and annexin-II (Zhao et al., 2010; for the purpose of retinal neovascularization and (Chan-Ling et al., 2004) and membrane domain organization and endosome internalization (Gerke et al., 2005)). The 21-residue transmembrane domains contains an orthologically-conserved hydrophobic sequence and single charged glutamic acid responsible for mediating interaction with cyclophilin 60 (a folding and ER to membrane trafficking chaperone of basigin) (Pushkarsky et al., 2005), syndecan-1 (a basigin complex partner and chaperone of cyclophilin B-mediated chemotaxis/cell adhesion; Pakula et al., 2007), and MCT-1,-4 (a membrane-bound extracellular effluxor of the anaerobic glycolysis byproduct lactic acid; Manoharan et al., 2006). Basigin's transmembrane domain also includes one leucine zipper motif which is responsible for facilitating homo- and heterodimeric protein interactions (Weidle et al., 2010). All isoforms have the characteristic (Ig)-like

extracellular domain two (i.e. the most-proximal extracellular domain to the cell surface; Liao et al., 2011) which along with basigin's cytoplasmic domain has been characterized to mediate interaction with caveolin-1, a negative regulator of basigin dimerization and receptor-mediated MMP production (Tang et al., 2004). The medially-located extracellular domain to the cell surface, domain one, is responsible for mediating basigin dimerization and MMP induction in neighboring fibroblasts (Yoshida et al., 2000) when it is highly glycosylated (Tang et al., 2004).

Tissue-specific expression of basigin's isoforms is tissue-specific. Basigin-1 is a retinal-specific isoform whose function is to dimerize and interact with MCT-1 for lactic acid export-mediated intracellular pH stability (Hanna et al., 2003). A 2011 study by Liao et al. analyzed human hepatocellular carcinoma and adjacent normal tissue to observe high expression levels of basigin-2 in heart, kidney, skeletal muscle, and testis with basigin-3 and -4 having high expression in bone marrow, fetal liver, lung, testis, and thymus tissues. While all isoforms localized to the plasma membrane to form dimers, basigin-2 mRNA expression levels within normal tissues were on average 1,300 and 6,600-fold greater than for basigin-3 and -4, respectively. Similarly, basigin-2 and -3 mRNA levels in the hepatocellular carcinoma samples were significantly greater than that of adjacent normal tissues (Liao et al., 2011). Prior to post-translational modification basigin-2 resolves on sodium dodecyl-sulfate polyacrylamide gel electrophoresis as a 29 kDa protein. As with all basigin isoforms, the degree of post-translational N-linked β1,6-branched polylactosamine glycosylation (Dennis et al., 1999) heavily influences basigin-2 to result in 39 (low-glycosylated to 65 (high glycosylated) kDa mass (Weidle et

al., 2010) via its three asparagine glycosylation sites. In malignant breast cancer cells, basigin-2 is expressed and promotive of tumor growth and metastasis (Zucker et al., 2001) with its caveolin-influenced (Tang et al., 2004) glycosylation level influencing its MMP-production ability (Dennis et al., 1999). Sp1 promoter hypomethylation and activity has been shown to influence basigin over-expression and induce poor prognosis in some cancers (Kong et al., 2011). Basigin-2 is also expressed on circulating tumor cells (Pituch-Noworolska et al., 2007) and primary ovarian cancer stem cells following CD133+ enrichment (Slomiany et al., 2009). Clearly, basigin-2 expression is highly upregulated in cancerous tissue and most-likely important in maintaining chemoresistance, invasiveness, and tumorigenicity (Dai et al., 2013).

Tumorigenesis relies on the ability to alter the local tumor microenvironment which includes ECM constituted of carbohydrates, factors, and proteins. Basigin can induce soluble and membrane-type MMPs (MT-MMPs) in adjacent tissue to degrade the ECM and allow for cancer cell migration. The interaction between basigin-2 and CD44, a cell-surface receptor for an extracellular glycosaminoglycan, has been well studied and deemed responsible for mediating tumor invasion and chemoresistance (Reviewed by Grass et al., 2014). One of basigin-2's influence on tumorigenesis is through the plasma membrane receptor CD44 which is also localized to plasma membrane lipid raft domains (Murai et al., 2011**;** Oliferenko et al., 1999). A major component of the ECM is the linear nonsulfated glycosaminoglycan hyaluronan acid which interacts with CD44 to mediate various cellular functions and stabilize lipid raft complexes on the cell surface (Grass et al., 2014). Metastasis is mediated by basigin-2/CD44 complexes which drive the

epithelial-mesenchymal transition (EMT) of the cancer cell to allow for release of cell-cell contacts and anchorage independent growth (anoikis), cytoskeletal rearrangement, and antiapoptotic signaling events (Kalluri & Weinberg, 2009; Teng et al., 2007). Extracellular lactic acid stimulates the production of HA (Stern et al., 2002) which stabilizes CD44, and HA regulates EMT (Camenisch et al., 2000; Zoltan-Jones et al., 2003). Additionally, basigin-2 has been shown to stimulate the formation of cell-surface protrusion called invadopodia which are rich in membrane-bound lipid-rafts containing the protease MT1-MMP, CD44, and EGFR (epithelial growth factor receptor)(Grass et al., 2012). EGFR is mutated and constitutively active in some subtypes of GBM (Montano et al., 2011) which can lead to an increased level of ERK (extracellular signal-regulated kinase)-mediated cell-signaling events. Basigin-2 has also been shown to block annexin-II phosphorylation which contributes to mesenchymal-amoeboid-like movement necessary for EMT (Zhao et al., 2011). This complex within the lipid raft domain is stabilized by HA-CD44 interactions as well (Grass et al., 2012)**.** Basigin-2 also coordinates with CD55-HA complexes to stimulate PI3-kinase activity (Ghatak et al., 2005) which regulates expression of the ABC-family of drug transporters (ABCB1; Misra, Ghatak, & Toole, 2005). Basigin-2's role in facilitating MCT-shuttled lactic acid due to anaerobic glycolysis may stabilize and mediate CD44-HA cell-signaling cascades (Marieb et al., 2004) to promote tumor invasiveness and chemoresistance (Dai et al., 2013). Basigin-2 has also been shown to influence neovascularization through a VEGF mediated mechanism (Voigt et al., 2009) as discussed above.

Taken together, basigin-2 is a transmembrane peptide with biological function and relevance in various physiological and pathological conditions. Its ability to serve as a mediator and receptor for various ligands to influence various signaling pathways, capability to be biologically relevant when soluble extracellularly, and ability to bind homophilically has identified basigin-2 as a novel target for specifically demarcating or treating tumor cells. Belton et. al has shown that a 25 kDa prokaryotic-expressed soluble recombinant extracellular domain of basigin-2 (rBSG-2), consisting of basigin-2's non-glycosylated extracellular domain, is able to form dimers in solution and be internalized by uterine fibroblasts to activate downstream signaling and expression of MMP-1, -2, and -3 (2008). Thus, the goal of this project was to characterize various recombinant peptides for future use as tumor-specific treatment vehicle with innate antitumor activity.

HYPOTHESIS, AIMS, & OBJECTIVES

Hypothesis 1: The efficacies of fluorescent-labelled recombinant chlorotoxin (rCTX) and recombinant extracellular basigin-2 (rBSG-2) as therapeutic vectors specific for adherent GBM cells differs.

Aim 1.1: Characterize rCTX temporal labelling of GBM cells *in vitro*.

Objective 1.1: Create rCTX in an *E. coli* expression system.

Objective 1.2: Fluorescently label rCTX with Alexafluor-488.

Objective 1.4: Perform confocal microscopy for visual indication of rCTX-mediated temporal cell labelling.

Aim 2.1: Characterize rBSG-2 temporal labelling of GBM cells *in vitro.*

Objective 2.1: Express and fluorescently-label rBSG-2 with Alexafluor-488.

Objective 2.2: Perform confocal microscopy for visual indication of rBSG-2-mediated temporal cell labelling.

METHODS

Purification of Recombinant Basigin-2 (rBSG)

Gifted from Dr. Robert Belton (Northern Michigan University) were transformed BL21-RP Codon-Plus *Escherichia coli* (Agilent, formerly Stratagene) harboring the pASK_IBA44 (IBA, Cat. 2-1344-000) periplasmic bacterial expression vector containing the extracellular domain of human basigin, amino acids 23-206 of isoform 2 (BL21-rBSG). Recombinant protein expression was completed as described by Belton et al. (2008). Specifically, a glycerol stock of BL21-rBSG was streaked onto a LB Agar plate containing 100 μg/mL ampicillin and 50 μg/mL chloramphenicol (AGAR/A/C). Following culture for 13 hours at 37 °C, a single bacterial colony was used to inoculate 5 mL of SOC medium (2% tryptone (BD, Ref. 211705), 0.5% yeast extract (Difco, Cat. 212750), 10 mM NaCl (Fisher Scientific, Cat. BP358-1), 2.5 mM KCl (Fisher Scientific, Cat. P-217), 10 mM $MgCl_2$ (Fisher Scientific, Cat. M33-500), and 20 mM glucose (Gibco, Cat. 15023-021)) containing 100 μg/mL ampicillin and 50 mL chloramphenicol (SOC/A/C). The culture was grown for 5 hours at 37 °C and 250 RPM, diluted 1:50 into SOC/A/C, and grown for 12 hours at room temperature and 200 RPM. Cultures were diluted 1:4 into SOC containing 100 μg/mL ampicillin (SOC/A) and grown for 1 hour at room temperature and 200 RPM. Protein expression was induced with 0.2 μg/mL anhydrotetracycline (2 mg/mL in dimethyl formamide stock suspension) for 5 hours to reach A_{550} >0.8. Detergent-free osmotic shock lysate (OSL) containing periplasmic-expressed recombinant peptide was then obtained and kept on ice for the remainder of the procedure. For this, the culture was centrifuged for 10 minutes at 3,220 x g and 4 °C, and

the cell pellet was resuspended in ice-cold sucrose buffer (20% sucrose, 30 mM Tris, pH 8.0) at a concentration of 60 mL/g of wet weight pellet. Following plasmolysis and separation of the plasma membrane from the cell wall, 1 mM ice-cold EDTA was added dropwise and incubation occurred on ice for 10 minutes. The sucrose supernatant was discarded after 20 minutes of 4 °C centrifugation at 3,220 x g. Bacterial pellet was resuspended with equal volume of ice-cold 5 mM $MgSO_4$ and incubated on ice for 10 minutes to induce cytolysis and removal of periplasmic content from the cell. OSL containing recombinant peptide was obtained and kept on ice after 3,220 x g centrifugation for 20 minutes at 4 °C. To prepare for rBSG purification, OSL was filtered through a 0.45-μm cellulose acetate membrane filter (VWR, Cat. 28145-481) to remove cellular debris. OSL was concentrated 50:1 via multiple 20 minute 3,220 x g centrifugations at 4 °C with 10-kDa centrifugal filters (Amicron, Cat. UFC501024). Prior to peptide affinity purification, 1x wash buffer (300 mM NaCl, 50 mM NaH_2PO_4, pH 8.0) was added to reduce the concentration of $MgSO_4$ within the concentrated OSL to <0.1 μM and reconcentrated via multiple centrifugal filtrations at 3,220 x g and 4 °C for 20 minutes. The OSL obtained from 1 liter of culture was incubated with 1 mL of 50% (v/v) Co-NTA resin (GBiosciences, Cat. 786-286) in 1x wash buffer for 12 hours at 4 °C while on slow rotation. Following incubation, the resin was pelleted by centrifugation at 1000 x g for 1 minute at 4 °C and unbound protein was removed. A Co-NTA wash of the resin was performed with 30 bed volumes of Co-NTA buffer (wash buffer containing 5 mM imidazole and 0.5 mM phenylmethylsulfonyl fluoride (PMSF). Following resin centrifugation, the elution column was then moistened with 30 bed volumes of deionized water and 2 bed volumes of wash buffer prior to transfer of the resin/10 bed volume Co-

NTA slurry to the elution column. Excess 1x wash buffer was used to transfer remaining resin into the elution column. Once the resin was settled, the column wash was completed by draining the elution column. Elution of purified recombinant protein from the resin was obtained in five 1 mL fractions with 10 bed volumes of elution buffer containing wash buffer, 200 mM imidazole, and 0.5 mM PMSF. Samples of eluted protein, wash steps, "unbound," and OSL were saved for characterization by sodium dodecyl sulfate polyacrylamide gel electrophoresis (SDS-PAGE).

Generation of Recombinant Chlorotoxin (rCTX) Construct

Purified pASK_IBA44 (IBA, Cat. 2-1344-000) periplasmic bacterial expression vector was transformed into E. cloni 10G *Escherichia coli* (Lucigen, Cat. 60106) by following the provided protocol. A transformed clone was then expanded in LB culture medium prior to plasmid purification with Plasmid Maxi Kit (Qiagen, Cat. 12163). All plasmid purifications were performed with 30 mL glass oakridge tubes (Corex, Cat. 8445), a SS-34 Sorvall rotor, and Sorvall RC 5B Plus centrifuge. The novel nucleic acid sequence for rCTX was codon optimized with GeneScript online tool (http://www.genscript.com/cgi-bin/tools/codon_freq_table) after being extrapolated from the CA4 amino acid sequence published by Xu et al. (2016; Figure 4A). The pUCIDT MiniGene plasmid (IDT) containing the rCTX nucleotide sequence flanked by BsaI endonuclease recognition sites was transformed into E. cloni 10G *E. coli* cells. A transformed clone was then expanded in LB culture medium prior to plasmid purification with Plasmid Midi Kit (Qiagen, Cat. 12143). Following the provided protocol, purified pUCIDT MiniGene plasmid containing the rCTX oligo and pASK_IBA44 vector were

digested with BsaI (New England Biolabs, Cat. R0535S) endonuclease and electrophoresed through a 1.2% agarose gel made with 1x TAE for 90 and 75 minutes, respectively, at 100 volts. Gel purification of rCTX oligo and linearized plasmid vector were performed with the QIAquick Gel Extraction Kit (Qiagen, Cat. 28704). Ligation of purified rCTX oligo and pASK_IBA44 plasmid vector for poly-histidine tag purification was performed at an oligo to vector ratio of ~12:1 with Quick Ligase (New England Biolabs, Cat. M2200). Transformation of pASK_IBA44/rCTX construct into E. cloni 10G *Escherichia coli* (Lucigen, Cat. 60106) was performed, and transformed clones were selected and expanded in LB culture prior to plasmid purification with Plasmid Mini Kit (Qiagen, Cat. 12123). Purified pASK_IBA44/rCTX and purchased primers from IDT (Coralville, IA) (Figure 2D) were submitted to GeneWiz (South Plainfield, New Jersey, USA) for pre-defined Sanger sequencing and analyzed using SnapGene software (GSL Biotech, LLC., USA).

Transformation of BL21 with pASK_IBA44/rCTX Construct

Purified non-linearized pASK_IBA44/rCTX plasmid was transformed into BL21 competent *E. coli* (New England Biolabs, Cat. C2530H). Specifically, 40 µL of BL21 was thawed on ice for 10 minutes in a 1.5 mL Eppendorf tube. At this point, 1.3 ug of purified pASK_IBA44/rCTX or 50 pg of pUC19 control plasmid was added to tube, gently flicked, and allowed to incubate on ice for 30 minutes. Heat-shock transformation was performed in a 42 °C water bath for 90 seconds. The tube was then immediately, and without agitation, placed in ice for 5 minutes followed addition of 960 µL of supplied room-temperature SOC medium. Transformation outgrowth was completed at 37 °C

while on rotation at 250 RPM for 60 minutes. LB agar plates were then streaked, incubated at 37 °C overnight, and colonies chosen for downstream protein purification.

Purification of Histidine-tagged rCTX

Purification of both soluble and insoluble rCTX was performed. Soluble rCTX was purified by streaking a glycerol stock of BL21 competent *E. coli* harboring the pASK_IBA44/rCTX construct onto a LB Agar plate containing 100 μg/mL ampicillin (AGAR/A). Following culture for 13 hours at 37 °C, a single bacterial colony was used to inoculate 5 mL of SOC medium containing 100 μg/mL ampicillin. The culture was grown for 5 hours at 37 °C and 250 RPM, diluted 1:50 into SOC/A, and grown for 12 hours at room temperature (21°C) and 200 RPM. Cultures were diluted 1:4 into SOC/A and grown for 30 minutes at room temperature and 200 RPM. Protein expression was induced with 0.2 μg/mL anhydrotetracycline (2 mg/mL in dimethyl formamide) for 5 hours to reach A_{550} >1.5. Detergent-free OSL containing periplasmic-expressed recombinant peptide was then obtained and kept on ice for the remainder of the procedure. Bacteria culture exposed to 10 minutes of 3,220 x g centrifugation at 4 °C provided cell pellets for resuspension in ice-cold sucrose buffer (20% sucrose, 30 mM Tris, pH 8.0) at a concentration of 60 mL/g of wet weight pellet. Following plasmolysis and separation of the plasma membrane from the cell wall, 1 mM ice-cold EDTA was added dropwise and incubation occurred on ice for 10 minutes. The sucrose supernatant was discarded after 20 minutes of 4 °C centrifugation at 3,220 x g. Bacterial pellet was resuspended with equal volume of ice-cold 5 mM $MgSO_4$ and incubated on ice for 10 minutes to induce cytolysis and removal of periplasmic content from the cell. OSL

containing recombinant peptide was obtained and kept on ice after 3,220 x g centrifugation for 20 minutes at 4 °C. To prepare for soluble rCTX purification, OSL was filtered through a 0.45-μm cellulose acetate filter (VWR, Cat. 28145-481) to remove cellular debris. OSL was concentrated 50:1 via multiple 20 minute 3,220 x g centrifugations at 4 °C with 10-kDa centrifugal filters (Amicron, Cat. UFC501024). For peptide affinity purification, 1x wash buffer (300 mM NaCl, 50 mM NaH_2PO_4, pH 8.0) was used to reduce the 5 mM $MgSO_4$ within the concentrated OSL to <0.9 μM via multiple centrifugal filtrations at 3,220 x g and 4 °C for 20 minutes. The OSL obtained from 1 liter of culture was incubated with 1 mL of 50% (v/v) Co-NTA resin (GBiosciences, Cat. 786-286) in 1x wash buffer for 12 hours at 4 °C while on slow rotation. Following incubation, the resin was pelleted by centrifugation at 1000 x g for 1 minute at 4 °C and unbound protein was removed. A Co-NTA wash of the resin was performed with 30 bed volumes of Co-NTA buffer (wash buffer containing 5 mM imidazole and 0.5 mM phenylmethylsulfonyl fluoride (PMSF). Following resin centrifugation, the elution column was then moistened with 30 bed-volumes of deionized water and 2 bed volumes of wash buffer prior to transfer of the resin/10 bed volume Co-NTA slurry to the elution column. Excess wash buffer was used to transfer remaining resin into the elution column. Once the resin was settled, the column wash was completed by draining the elution column. Elution of purified recombinant protein from the resin was obtained in five 1 mL fractions with 10 bed volumes of elution buffer containing wash buffer, 200 mM imidazole, and 0.5 mM PMSF. Samples of eluted protein, wash steps, “unbound,” and OSL were saved for characterization by SDS-PAGE.

To assess the potential yield of purified and denatured rCTX from its insoluble form, a two-step denaturation process was performed. Frozen post- or non-induced cell pellet from 50 mL of culture was thawed on ice with 4 mL of ice-cold Buffer I (20 mM Tris, pH 8.0) for 10 minutes. Using the Model 500 Sonic Dismembrator (Fisher Scientific), sonication of thawed pellet was performed for ten 40 second intervals at 25% duty cycle while on ice. Insoluble rCTX inclusion bodies were obtained after a 30 minute centrifugation at 20,000 x g at 4 °C with a table-top centrifuge (Eppendorf model 5810R) and rotor (Eppendorf model FA-45-30-11). The supernatant was removed for SDS-PAGE analysis and insoluble rCTX pellet was incubated in 7.5 mL of room temperature Buffer II (50 mM Tris, 50 mM NaCl, 2% Triton X-100, 1.5 mM β-mercaptoethanol, 1.6 M urea, pH 8.0) at room temperature for 20 minutes while on slow rotation. Centrifugation at 20,000 x g at 4 °C followed and the insoluble rCTX pellet was subjected to incubation with Buffer II and centrifugation once more. Pure rCTX inclusion bodies from 50 mL of culture were incubated in 250 μL of room temperature Extraction Buffer I (50 mM Tris, 50 mM NaCl, and 6 M GdnHCl, pH 8.0) at room temperature for 10 minutes. The supernatant obtained from the following 30 minute centrifugation at 20,000 x g and 4 °C was diluted into 10 mL of room temperature Dilution Buffer (50 mM Tris, 50 mM NaCl, 1.5 mM β-mercaptoethanol, and 1 mM EDTA) to rapidly precipitate rCTX inclusion bodies over a 10 minute room temperature incubation. The contents were centrifuged at 20,000 x g and 4 °C for 30 minutes followed by suspension of the pellet in 250 μL of room temperature Extraction Buffer II (50 mM Tris, 50 mM NaCl, and 8 M urea, pH 8.0) and incubation at room temperature while on slow rotation for 20 minutes. A final centrifugation at 20,000 x g and 4 °C for 30 minutes produced supernatant containing

solubilized inclusion bodies of rCTX. Samples from select purification steps were saved for SDS-PAGE analysis.

To further assess the potential yield of purified/denatured rCTX from inclusion bodies, a one-step 30 minute or 16 hour denaturation period was performed prior to batch purification. Frozen post- or non-induced cell pellets from 50 mL bacterial culture were thawed in 10 mL of room temperature Denaturation Buffer (20 mM Tris, 8 M urea, 10 mM DTT, pH 8.0) and sonicated for ten 40 second intervals at 25% duty cycle while on ice. The whole cell lysate (WCL) was then incubated for 30 minutes or 16 hours at 37 °C while on slow rotation. Centrifugation of WCLs at 20,000 x g for 30 minutes and 4 °C provided supernatant containing soluble rCTX. Solubilized rCTX was passed through a 0.2 μm cellulose acetate membrane filter (VWR, Cat. 28145-477) to remove cellular debris. Batch purification of rCTX was performed by adding 100 μL of 50% (v/v) Co-NTA resin (GBiosciences, Cat. 786-286) in 1x wash buffer for 12 hours at 4 °C while on slow rotation. Following incubation, the resin was pelleted by centrifugation at 1,000 x g for 1 minute at 4 °C and unbound protein was removed. Unbound urea-soluble WCL supernatant was removed from the resin after it had settled for 2 hours at room temperature and had been centrifuged at 1000 x g for 1 minute at room temperature. Co-NTA resin bound to rCTX was then incubated/washed with 500 μL of Co-NTA buffer for 5 minutes at room temperature and resin pelleted by centrifugation at 1,000 x g for 5 minutes at room temperature. The supernatant was removed for analysis and 150 μL of Elution Buffer was added and incubated for 5 minutes at room temperature with the Co-NTA resin. A 1,000 x g centrifugation for 5 minutes at room temperature was performed

to pellet the Co-NTA resin for decanting of the eluted rCTX. In total, four consecutive elutions were performed. Samples from all purification steps were saved for SDS-PAGE analysis.

Characterization of Purification Samplings and Recombinant Peptides

Purified recombinant protein and samples from all purification steps were analyzed by SDS-PAGE. A 4-15% SDS-PAGE gel (Bio-Rad, Cat. 456-1084) was resolved for 60 minutes at 100 volts in 1x Tris/Glycine (Bio-Rad, Cat. 161-0772). A Bio-Rad Mini-PROTEAN Tetra System and Bio-Rad Power Pac 300 Unit were utilized. A 250 to 10 kDa ladder (Bio-Rad, Cat. 161-0374) was used, of which 5 μL was loaded. The 30 μL SDS-PAGE samples containing 1x Laemmeli sample buffer (LSB) and 25 mM DTT were incubated at 95 °C for 5 minutes, vortexed, and centrifuged at 1,000 x g for 1 minute prior to loading. Following electrophoresis, the SDS-PAGE was stained with 0.1% coomassie blue R250 in 10% glacial acetic acid and 50% methanol solution at room temperature and 50 RPM. Once completely stained, the SDS-PAGE gel was destained with 10% glacial acetic acid and 50% methanol solution for 3 hours and thrice washed with tap water before being soaked in tap water for 90 minutes to rehydrate the gel. Imaging was performed, and the photo negative was analyzed due to increased picture clarity. In using ImageJ, the relative background-normalized densitometry score was quantified as compared to lane one of the gel to characterize sample protein content patterns.

Conjugation of Peptide to Alexa-fluor 488

Purified rBSG in Elution Buffer was desalted by phosphate buffered saline (PBS; Lonza, Cat. 17-516). Multiple centrifugations with purified rBSG and PBS were performed with a 10-kDa centrifugal filters (Amicron, Cat. UFC501024) for 50 minutes at 3,220 x g and 4 °C. Reduction of salt and solute concentration by a factor of 7,2000:1 eliminated any possible non-peptide influence on bicinchoninic acid analysis (BCA) and conjugation of rBSG with fluorescent marker. The Pierce BCA Protein Assay Kit (Thermo Scientific, Cat. 23225) was used to determine rBSG protein concentrations. One milligram of lyophilized CTX (Alamone Labs, Cat. RTC-450) was suspended in PBS (Lonza, Cat. 17-516) to create a 2 mg/mL suspension. Conjugation of 1 mg (2 mg/mL) rBSG and CTX to Alexa Fluor 488 (AF488) was accomplished with the labelling kit (Thermo Scientific, Cat. A20181). Purification of labelled peptide from fluorophore was performed under dark and sterile conditions. An 18.5-gauge needle (BD, Cat. 305196) and 1 mL syringe (BD, Cat. 309602) was used to inject labelled peptide into a moistened 0.1-0.5 mL, 3.5 molecular weight cut off (MWCO), dialysis float (Thermo Scientific, Cat. 66330) for dialysis into 500 mL of sterile PBS (Lonza, Cat. Cat. 17-516) for 13 hours. This was repeated for a second time. Upon completion of dialysis, 50 µL aliquots of 2 mg/mL AF488-labelled peptide (i.e. CXT-AF488; rBSG-AF488) were created and stored at -80 °C.

Cell Lines and Reagents

The adherent glioblastoma cell line U87 was obtained from the American Type Culture Collection and cultured to their accordance, without antibiotics; 5 minute

centrifugation at 200 x g and 4 °C was used to pellet cells. Immortalized human foreskin fibroblasts (Morgan et al., 1991) were provided by Justin McCormick (Michigan State University) and cultured under the same methods and conditions as U87.

In Vitro Cell Labelling Assay

U87 or MSU1.1 cells in 8-chamber culture slides (BD Falcon, Cat. 354118) were seeded with 300 μL of complete media containing 50,000 colony forming units (CFU; i.e. cells) for 12 hours. Complete media was then aspirated and 250 μL of serum-free (SF)-EMEM containing 5 μM CTX-AF488 or rBSG-AF488 or SF-EMEM-only was dispensed and allowed to incubate for 30 minutes under normoxic conditions. Each culture slide was treated with peptide, in duplicate, and SF-EMEM-only in quadruplet. Following treatment, all 8 of the chambers on the culture slide were aspirated of media and replaced with equal volume of SF-EMEM. Post-treatment incubation under normoxic conditions for either 30 minutes, 6 hours, or 24 hours then occurred. Following post-treatment incubation of 8-chamber culture slides, medium was aspirated, and chambers were washed with 250 μL of warm PBS (Lonza, Cat. 17-516). The labelled or control cells on each slide were then fixed for 45 minutes with 250 μL of 4% paraformaldehyde (PFA) at room temperature. Following aspiration of PFA, a wash with 250 μL of PBS (Lonza, Cat. 17-516) was performed. Removal of the chamber from the slide was performed as described by its product-supplemented protocol. Finally, all chambers in each slide received 1 drop of chilled Prolong diamond Antifade Mountant with Dapi (Thermo Fisher Scientific, Cat. P36962) before being coverslipped and allowed to cure for 24 hours prior to imaging.

Confocal Microscopy and Image Analysis

Representative 60x images from each treatment condition were obtained using Olympus FLUOVIEW FV1000 laser scanning confocal microscope. A scanning speed of 20 μs/pixel and aspect ratio of 800 X 800 were employed. The nuclear counterstain DAPI (Ex. 405 nm, Em. 461 nm) and green fluorescent dye AF488 (Ex. 490 nm, Em. 525 nm) were used. Imaging parameters between control and treatment conditions for each time point and peptide application were kept constant.

RESULTS

Purification of rBSG

As previously described by Belton et. al (2008), the non-glycosylated extracellular domain of basigin-2 (abbreviated rBSG) was expressed and purified. Briefly, expression of soluble rBSG was directed to the non-reductive prokaryotic periplasmic space to ensure proper formation of disulfide bonds crucial to proper extracellular (Ig)-like domain development. Following induction of rBSG expression, *E. coli* were osmotically shocked to obtained only periplasmic content (OSL). OSL containing histidine-tagged rBSG was centrifugally concentrated and desalted prior to purification via immobilized metal ion affinity chromatography (IMAC). Binding of rBSG to 6x-histidine tag to cobalt-coated agarose resin facilitated flow-through of non-histidine-tagged proteins. Washing of chromatography column eliminated non-specific binding of cobalt-coated agarose resin to histidine and cysteine side chains of non-target proteins. Elution of target rBSG protein from IMAC was performed with imidazole, a histidine analog with high-affinity to cobalt ions. All sample fractions were obtained and electrophoresed on SDS-PAGE (Figure 1). A ~ 25 kDa band is present in all SDS-PAGE lanes. Successive lanes indicate increasing intensity of ~ 25 kDa banding and simultaneous decrease in all other banding signal.

Generation of rCTX Construct

The CA4 peptide sequence generated by Xu et al. (2016; Figure 2A) was used to derive a novel DNA sequence for rCTX. The novel nucleic acid sequence for rCTX was

codon-optimized for bacterial expression of rCTX (Figure 2B). The oligonucleotide rCTX sequence (Figure 2C) is flanked by BsaI endonuclease recognition sites (Figure 5) and sourced via a pUCIDT MiniGene plasmid (IDT, Coralville, IA) for downstream use. BsaI-mediated linearization of purified pASK_IBA44 empty periplasmic expression vector and digestion of pUCIDT MiniGene plasmid containing the rCTX oligo was performed (Figure 3 and 4, respectively). Following pASK_IBA44 linearization, a ~ 3,300 b.p. band was observed (Figure 3). Following linearization of the pUCIDT MiniGene plasmid containing the rCTX oligo, a ~ 133 b.p. product was observed (Figure 4). Gel purification of linearized pASK_IBA44 plasmid and rCTX oligo was performed prior to ligation of the two products. Figure 5 illustrates the putative ligation of rCTX oligonucleotide within the multiple cloning site (MCS) of pASK_IBA44 expression plasmid. Correct assembly of the rCTX expression vector was confirmed with primers supplied with the pASK_IBA44 expression plasmid (Figure 2D). Sanger sequencing of ligated and bacterial purified rCTX expression construct was performed and putative peptide sequence was obtained and determined to be ~ 6.5 kDa with SnapGene software (Figure 6).

Purification of rCTX

The pASK_IBA44/rCTX construct was transformed into BL21 *E. coli* for use as a recombinant protein expression system. Transformation efficiency of BL21 was incalculable as colonies were overgrown on the plate after streaking. This method was performed after prior attempts with the supplemental BL21 transformation protocol which failed to yield colonies on LB agar plates (data not included). Briefly, histidine-

tagged expression and purification of soluble rCTX via IMAC was performed as described for purification of soluble rBSG. Figure 7 depicts purification of soluble rCTX (~ 6.5 kDa). A ~ 6.5 kDa band was not observed in the osmotic shock lysate (OSL), washes, or elution fractions. Next, two-step solubilization of presumed rCTX inclusion bodies was obtained and analyzed via SDS-PAGE. Briefly, sonication and centrifugation of rCTX-induced and non-induced bacterial cells pellets was performed to obtain soluble and insoluble protein fractions. The induced insoluble pellet was treated with a 1.6 M urea solution and centrifugation, twice. Pure rCTX inclusion bodies were denatured with 6 M GdnHCL-containing Extraction Buffer I, centrifuged, and obtained supernatant diluted with Extraction Buffer I (absent of 6 M GdnHCL) to rapidly precipitate rCTX. A final incubation and centrifugation with Extraction Buffer II containing 8 M urea was performed to obtain solubilized rCTX in the supernatant. Figure 8 depicts select samples from the purification process.

Batch purification of inclusion bodies presumably containing insoluble rCTX was performed following various denaturation periods. Briefly, rCTX-induced and control bacterial pellets were sonicated and exposed to an 8 M urea solution for 30 minutes or 16 hours to obtain whole cell lysates (WCL). Supernatant obtained from centrifuged WCL was removed of cellular debris via filtration and incubated with IMAC Co-NTA resin for 12 hours. Batch purification of rCTX with Co-NTA resin was performed without a column. Subsequent centrifugation and wash of the resin occurred to yield soluble WCL unbound protein within the supernatant. Multiple elutions of soluble rCTX were obtained after incubation and collection of supernatant from the Co-NTA resin.

Figures 9 and 10 depict select samples from the purification workflows. A decrease in protein detection is observed with successive purification samples. No protein is visibly observed in the various elution fractions.

U87 and MSU1.1 Cell Labelling with Fluorescently-conjugated Peptide

To determine the ability, specificity, and duration of bacterially-expressed CTX- and rBSG-mediated cell labeling, Alexafluor-488 (AF488) green fluorescent probe was conjugated to the respective peptide. U87 GBM or immortalized human skin fibroblast (MSU1.1) control cell line was incubated for 30 minutes with serum-free media (SFM) only or that containing 5 μM of conjugated peptide. Removal of treatment media, PBS wash, and replacement with SFM for 30 minutes, 6 hours, or 24 hours ensued prior to fixation and coverslipping of culture slide for confocal microscopy. Treatment of fluorescently-conjugated peptide on various cell lines qualitatively depicts vary results. Figure 11 depicts U87 GBM cells (see blue-stained nuclei) treated with (green) CTX-AF488. Regardless of time point, a high background-to-probe signal is observed between treatment and control images. The same cell line treated subjected to rBSG-AF488 treatment resulted in distinct high-signal punctate surrounding blue nuclei which decreased with time (Figure 12). No punctate were present in non-treated controls, but background-to-probe signal between treatment groups for all three time points were equal. Labelling of MSU1.1 by CTX-AF488 in Figure 13 does not provide any observable signal when compared to control, regardless of time point. In contrast to this result, labelling of the same cell line with rBSG-AF488 (Figure 14) yielded strong

punctate and qualitatively significant signal adjacent to nuclei when compared to control. Regardless of time point, this signal decreased with time.

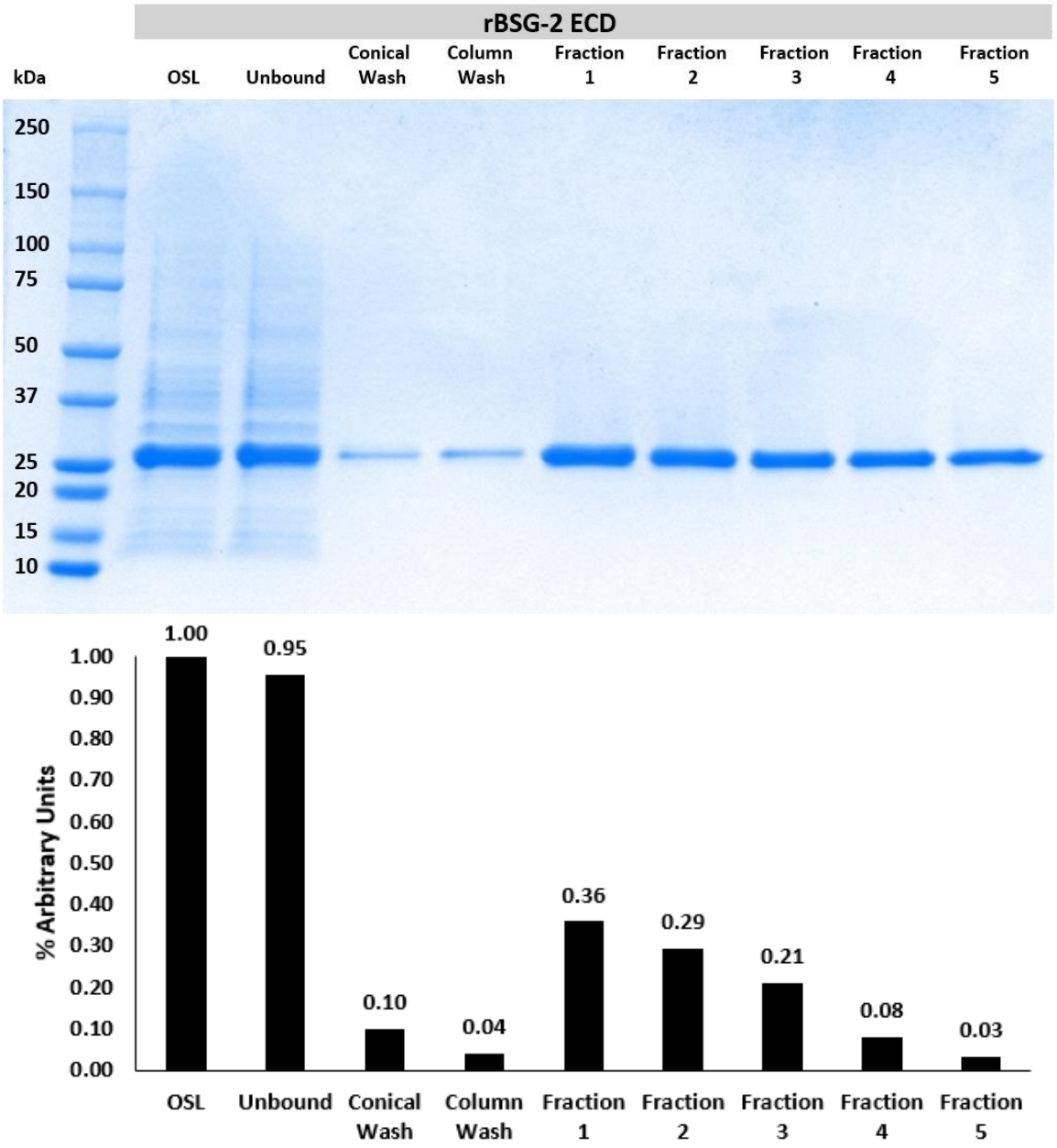

Figure 1. Purification of rBSG via Polyhistidine Tag. A 4-15% SDS-PAGE gel (Bio-Rad, Cat. 456-1084) was resolved for 60 minutes at 100V with a Bio-Rad Power Pac HC unit. A 250 to 10 kDa ladder (Bio-Rad, Cat. 161-0374) was used, of which 5 µL was loaded. The 30 µL SDS-PAGE samples (15 µL sample & 15 µL 2x LSB + 50 mM DTT) were heated at 95 °C for 5 minutes prior to loading. All samples were obtained from the IMAC-assisted purification of recombinant Basigin-2 extracellular domain (rBSG-2 ECD) protein. Fractions 1 through 5 were used for downstream ligation to fluorophore and subsequent use *in vitro*. Relative background-normalized densitometry score was quantified as compared to lane one

A

```
CTX  MCMPCFTTDHQMARKCDDCCGGKGRGKCYGPQCLCR 36 A.ACIDS
CA4  -CGPCFTTDHNMARKCDECCGGKGRGKCFGPQCLCR 35 A.ACIDS
```

B

	1				5					10
A.ACID	**M**	**C**	**G**	**P**	**C**	**F**	**T**	**T**	**D**	**H**
DNA	ATG	TGC	GGC	CCG	TGC	TTT	ACC	ACC	GAT	CAT
					15					**20**
	N	**M**	**A**	**R**	**K**	**C**	**D**	**E**	**C**	**C**
	ACC	ATG	GCG	CGT	AAA	TGC	GAT	GAA	TGC	TGC
					25					**30**
	G	**G**	**K**	**G**	**R**	**G**	**K**	**C**	**F**	**G**
	GGC	GGC	AAA	GGC	CGT	GGC	AAA	TGC	TTT	GGC
					35					
	P	**Q**	**C**	**L**	**C**	**R**				
	CCG	CAG	TGC	CTG	TGC	CGT				

C

```
5′ – GGTCTCGGCGCA[ATG]TGCGGCCCGTGCTTTACCACCGATCATAACATG
GCGCGTAAATGCGATGAATGCTGCGGCGGCAAAGGCCGTGGCAAATGCTTTGG
CCCGCAGTGCCTGTGC[CGT]GGCCGGAGACC – 3′
```

D

pASK_IBA44 Sequencing Primers:

```
Forward:  5′ – GAG TTA TTT TAC CAC TCC CT – 3′
Reverse:  5′ – CGC AGT AGC GGT AAA CG – 3′
```

Figure 2. Oligonucleotide and Peptide Sequences used for rCTX Peptide Generation. **A,** The CA4 peptide sequence generated by Xu et al. (2016) was used to derive a novel DNA sequence for rCTX. **B**, The novel nucleic acid sequence for rCTX was codon-optimized for bacterial expression of rCTX. **C**, The oligonucleotide sequence flanked by BsaI endonuclease recognition sites was ligated into a pUCIDT MiniGene plasmid (IDT, Coralville, IA); start and stop codons are bolded. **D**, The primers provided with the pASK_IBA44 (IBA, Cat. 2-1344-000) plasmid for sequencing following rCTX DNA ligation into empty vector.

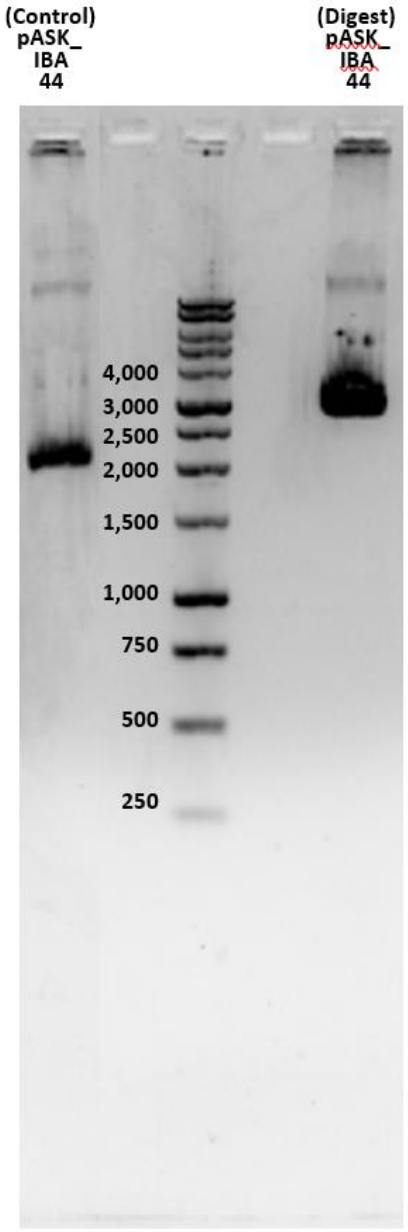

Figure 3. BsaI-mediated Linearization of pASK_IBA44. A 60 mL 1.2% agarose gel, made with 1X TAE and 1.2 μL EtBr, was resolved for 90 minutes at 100V. A 15 cm gel tray in a Fisher Biotech Electrophoresis System Mini-Horizontal Unit (# FB-SB-710) was used with a Bio-Rad Power Pac 300 unit. A 10,000 to 250 b.p. DNA ladder (1Kb, Promega, Cat. G571A) was used in lane 3, of which 5 μL was loaded. Of the Bsa1-digested sample, 1 μg was loaded. Of the undigested control, 0.5 μg was loaded. The inverted color image was obtained with a 2-second exposure. The linearization of pASK_IBA 44 periplasmic protein expression vector by BsaI indicates its suitable use for gel purification and ligation of rCTX oligonucleotide.

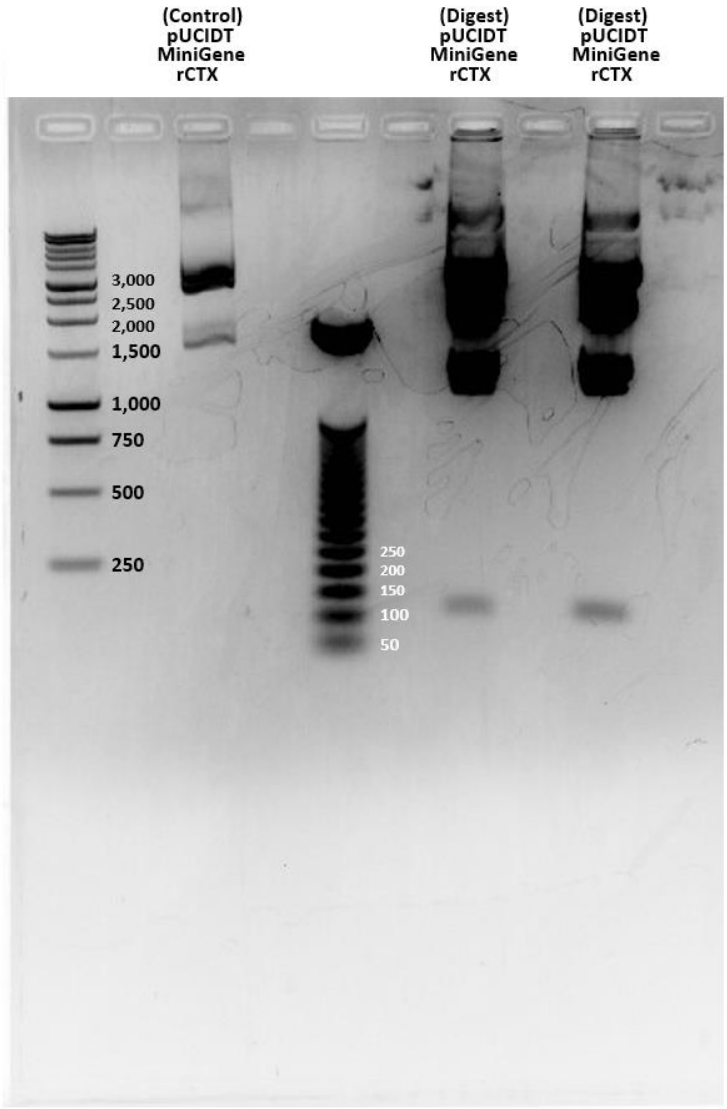

Figure 4. BsaI-mediated Digestion to Obtain rCTX Oligo. A 60 mL 1.2% agarose gel, made with 1X TAE and 1.2 µL EtBr, was resolved for 75 minutes at 100V. A 15 cm gel tray in a Fisher Biotech Electrophoresis System Mini-Horizontal Unit (# FB-SB-710) was used with a Bio-Rad Power Pac 300 unit. A 10,000 to 250 b.p. DNA ladder (1Kb, Promega, Cat. G571A) was used in lane 1, of which 5 µL was loaded. An 800 to 50 b.p. DNA Ladder (50 b.p. DNA Step Ladder, Promega, Cat. G452A) was used in lane 5, of which 5 µL plus 1 µL 6x Purple Loading Dye (New England Biolabs, Cat. B7024S) was loaded. Of the Bsa1-digested samples, 10 µg was loaded. Of the undigested control, 0.5 µg was loaded. The inverted color image was obtained with a 2-second exposure. **Note:** the ~130 b.p. bands in lanes 7 and 9 depict the rCTX oligonucleotide obtained with gel purification and ligation into pASK_IBA44 periplasmic expression vector.

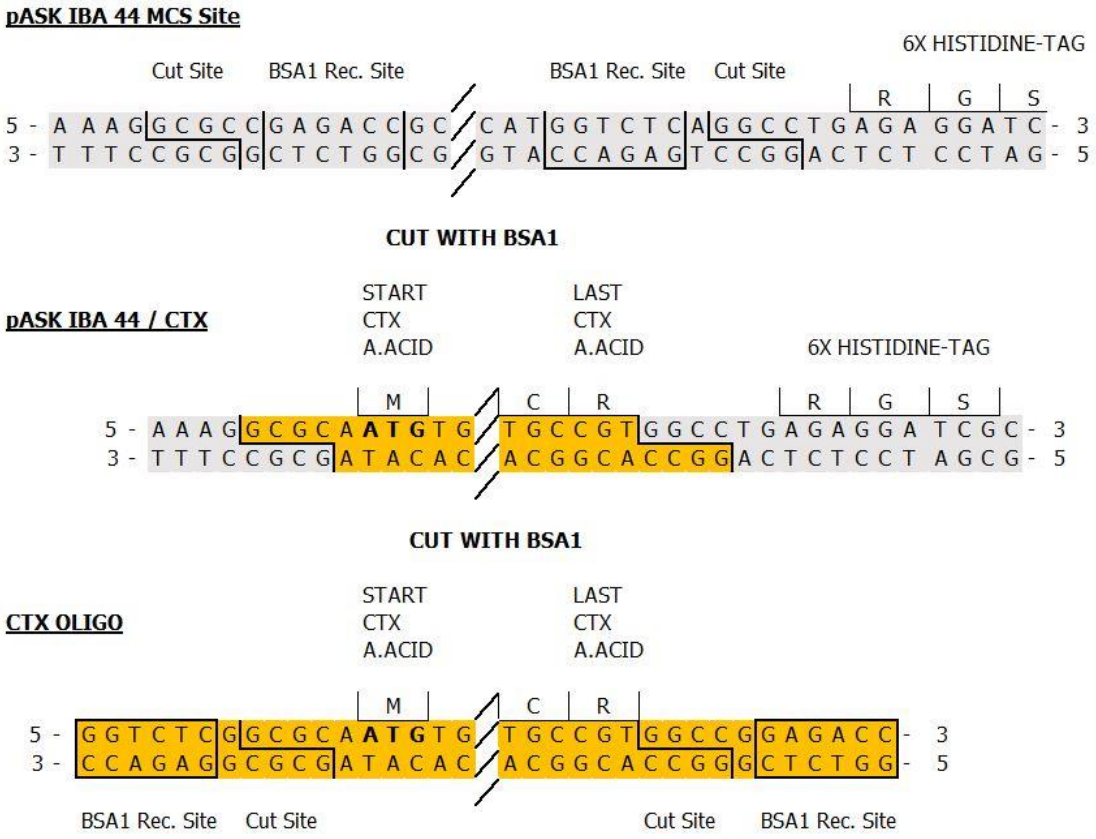

Figure 5. Bsa1-mediated Digestion and Ligation of rCTX Oligonucleotide. Illustrated in the BsaI endonuclease-mediated pUCIDT MiniGene donor plasmid to obtained rCTX oligonucleotide for ligation into the pASK_IBA44 (IBA, Cat. 2-1344-000) periplasmic vector for prokaryotic expression and purification.

Figure 6. Sanger Sequencing of the pASK_IBA44/rCTX MCS Containing rCTX. The ligated MCS needed for polyhistidine-tagged bacterial expression and purification of rCTX from BL21 *E. coli* was subjected to Sanger sequencing with pre-defined primers (provided with the pASK_IBA44 (IBA, Cat. 2-1344-000) periplasmic expression vector). Using SnapGene Viewer, the putative polypeptide product was determined to be ~ 6.5 kDa.

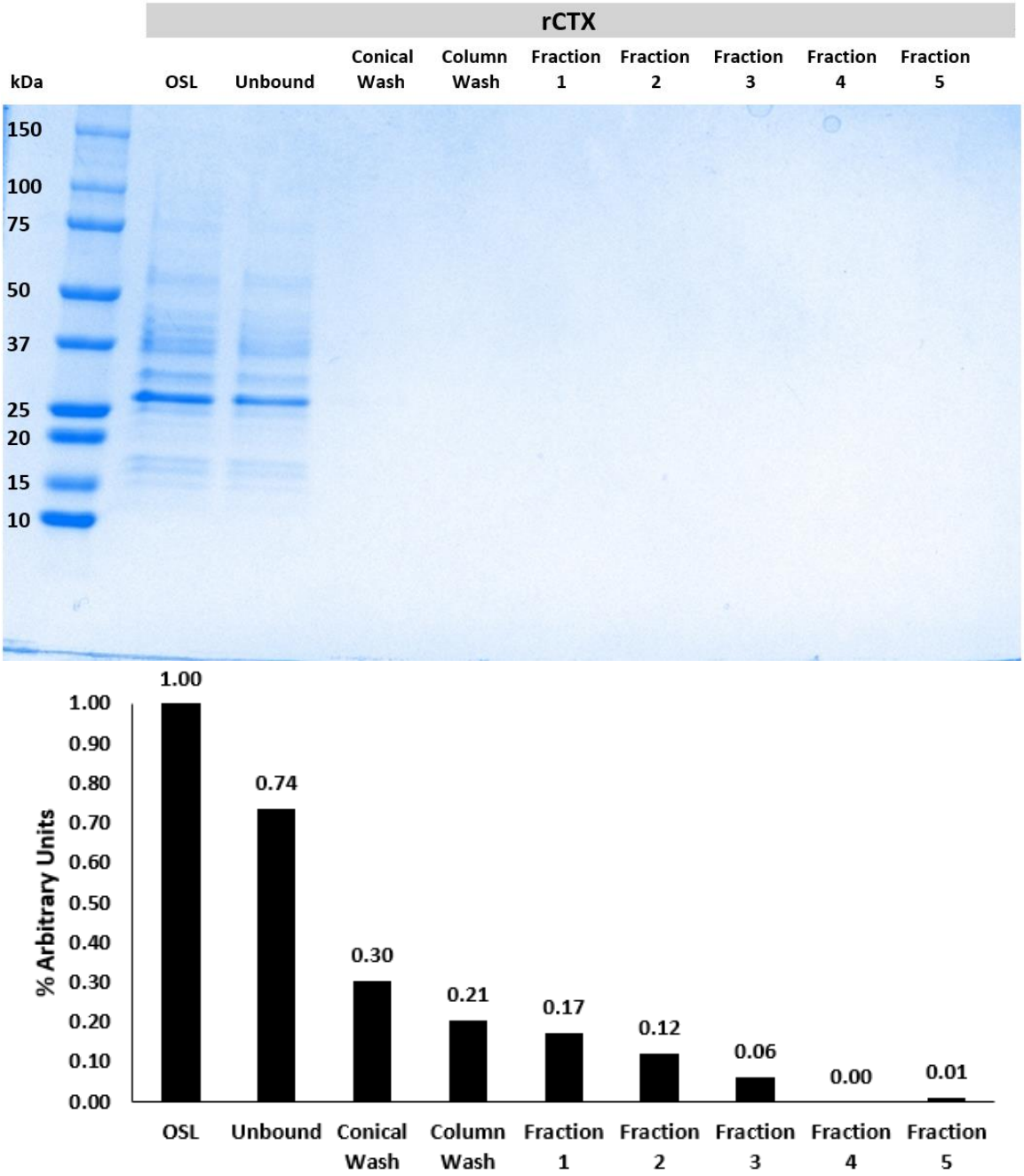

Figure 7. Purification of Soluble rCTX via Polyhistidine Tag. A 4-15% SDS-PAGE gel (Bio-Rad, Cat. 456-1084) was resolved for 62 minutes at 100V with a Bio-Rad Power Pac HC unit. A 250 to 10 kDa ladder (Bio-Rad, Cat. 161-0374) was used, of which 5 µL was loaded. The 30 µL SDS-PAGE samples (15 µL sample & 15 µL 2x LSB + 50 mM DTT) were heated at 95 °C for 7 minutes prior to loading. The expected rCTX product of ~ 6.5 kDa was not observed in the osmotic shock lysate (OSL), IMAC wash, or elution fractions which indicates that no soluble-expressed rCTX is expressed. relative background-normalized densitometry score was quantified as compared to lane one.

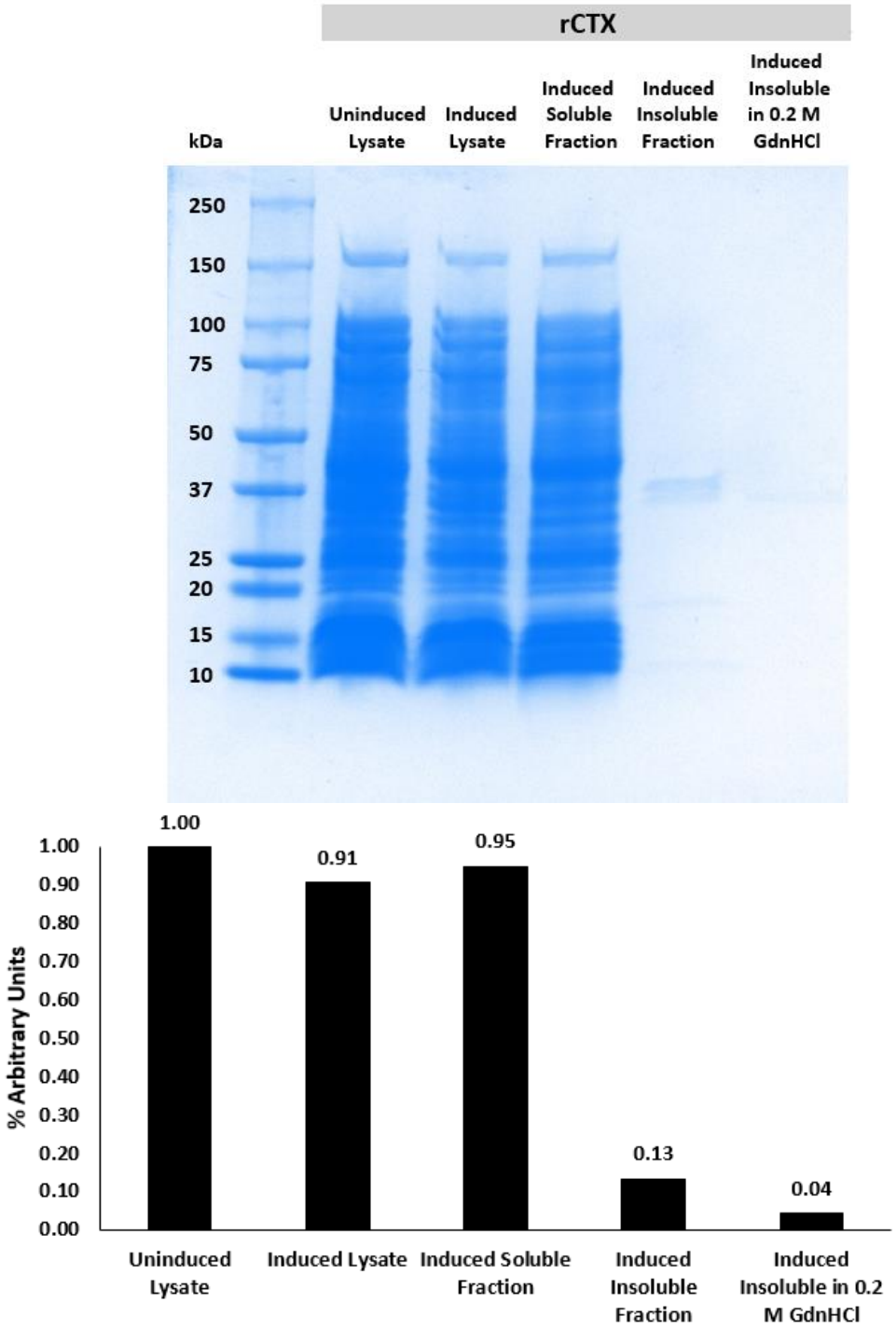

Figure 8. Two-step Denaturation of rCTX Inclusion Bodies. Following failed purification of soluble rCTX, purification of insoluble rCTx was attempted. Indicated by the absence of ~ 6.5 kDa banding in all lanes, two-step denaturation of bacterial inclusion bodies does not yield rCTX. IMAC purification of samples was not attempted because dilution of solubilized inclusion bodies to rapidly precipitate rCTX was unsuccessful. Relative background-normalized densitometry score was quantified as compared to lane one.

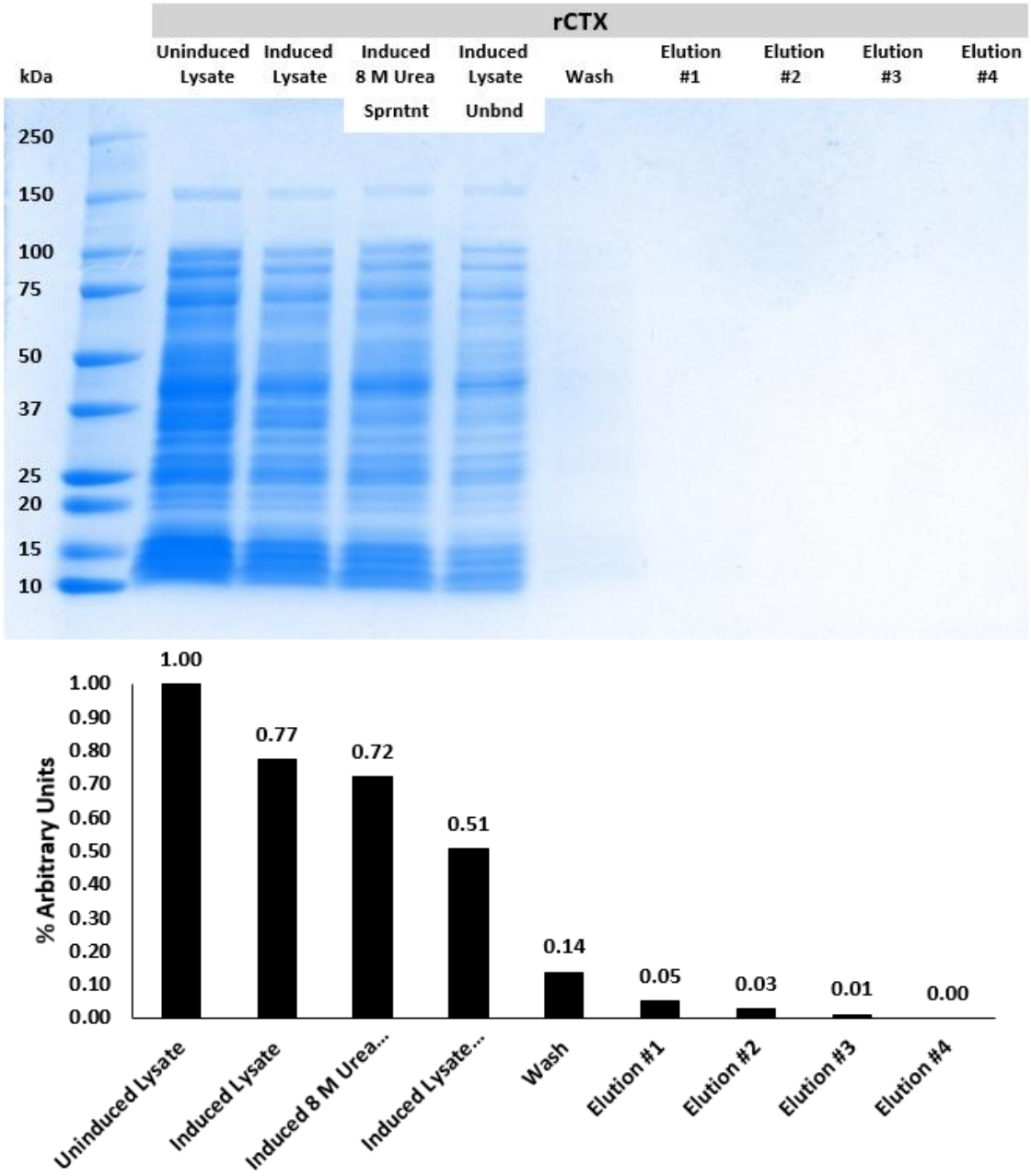

Figure 9. 30 Minute One-step Denaturation of rCTX Inclusion Bodies. A 4-15% SDS-PAGE gel (Bio-Rad, Cat. 456-1084) was resolved for 60 minutes at 100V with a Bio-Rad Power Pac 300 unit. A 250 to 10 kDa ladder (Bio-Rad, Cat. 161-0374) was used, of which 5 µL was loaded. The 30 µL SDS-PAGE samples (15 µL sample & 15 µL 2x LSB + 50 mM DTT) were heated at 95 °C for 5 minutes, vortexed, and centrifuged at 1,000 g for 1 minute prior to loading. The induced bacterial pellet was incubated in 20 mM Tris, 8 M urea, 10 mM DTT, pH 8.0 for 30 minutes at 37 °C prior to protein purification. Protein purification was performed via the "Batch Method." The absence of a ~ 6.5 kDa band in all lanes indicates that 30 minute one-step denaturation of bacterial inclusion bodies does not yield rCTX. Relative background-normalized densitometry score was quantified as compared to lane one.

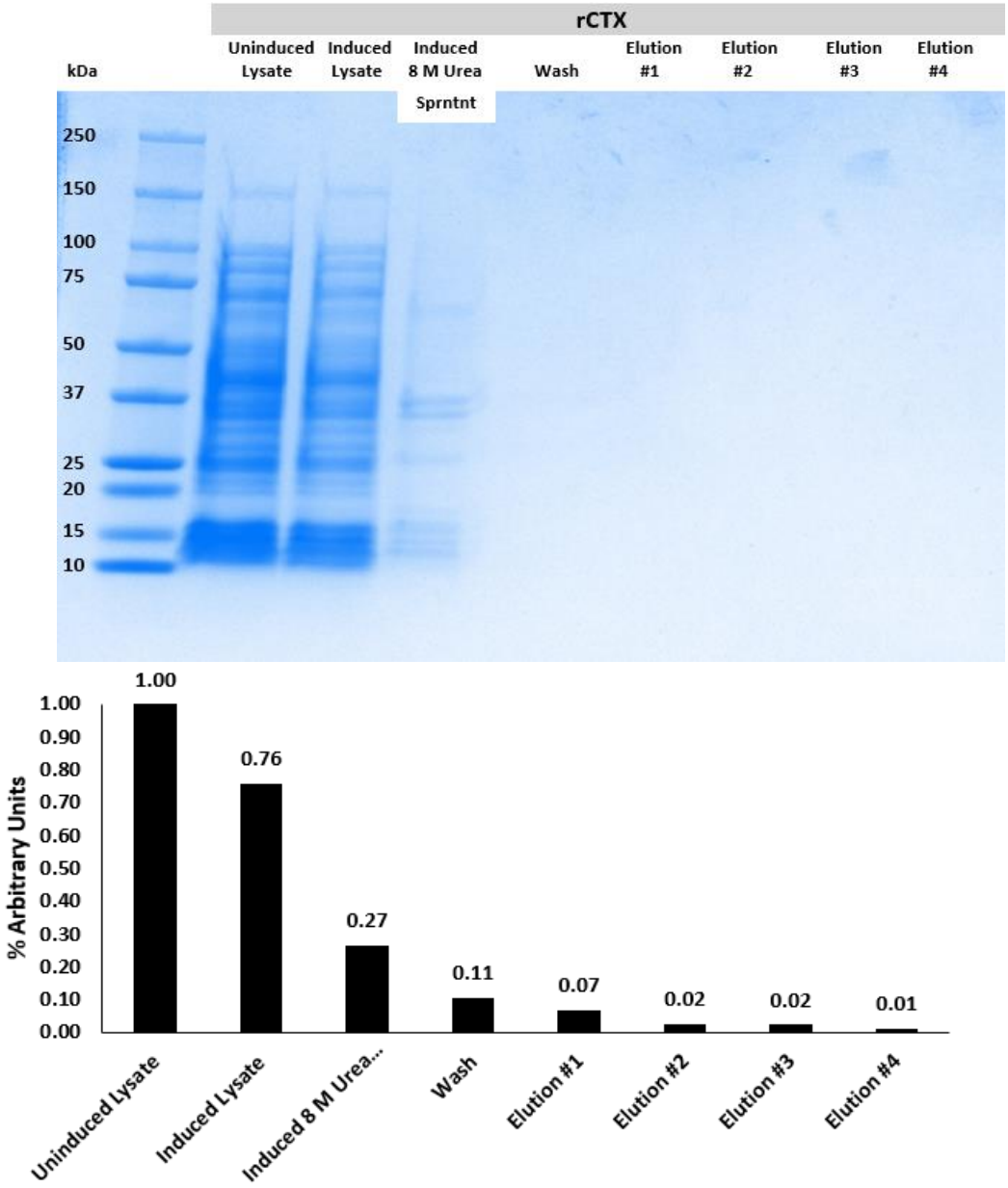

Figure 10. 16 Hour One-step Denaturation of rCTX Inclusion Bodies. A 4-15% SDS-PAGE gel (Bio-Rad, Cat. 456-1084) was resolved for 60 minutes at 100V with a Bio-Rad Power Pac 300 unit. A 250 to 10 kDa ladder (Bio-Rad, Cat. 161-0374) was used, of which 5 µL was loaded. The 30 µL SDS-PAGE samples (15 µL sample & 15 µL 2x LSB + 50 mM DTT) were heated at 95 °C for 5 minutes, vortexed, and centrifuged at 1,000 g for 1 minute prior to loading. Insoluble bacterial pellet was denatured for 16 hours at room temperature with shaking at 200 rpm. Pellet denaturation was performed with 8 M urea, 10 mM DTT, 20 mM Tris pH 8.0. Protein purification was then performed via the "Batch Method." The absence of a ~ 6.5 kDa band in all lanes indicates that 16 hour one-step denaturation of bacterial inclusion bodies does not yield rCTX. Relative background-normalized densitometry score was quantified as compared to lane one.

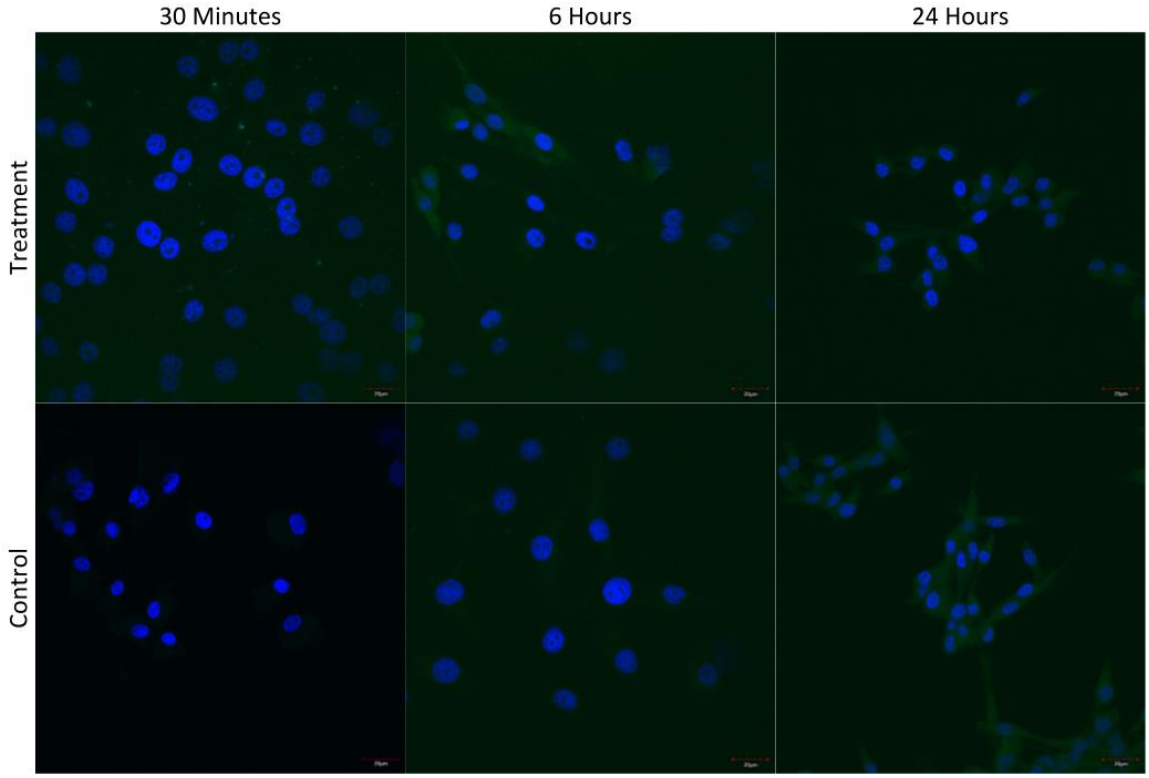

Figure 11. Labelling of U87 Cell Line with CTX-AF488. Serum-free EMEM media alone (i.e. control) or that containing CTX-AF488 was used to treat 50,000 CFU U87 GBM cells *in vitro* via 8-well chambered slides for 30 minutes under normoxic conditions. Post-treatment incubation under normoxic ensued for 30 minutes, 6 hours, or 24 hours prior to 4% paraformaldehyde fixation and imaging with confocal microscopy. An Olympus FLUOVIEW FV1000 laser scanning confocal microscope employed a scanning speed of 20 μs/pixel and 800 X 800 aspect ratio to obtain 60x images. The nuclear counterstain DAPI (Ex. 405 nm, Em. 461 nm) and green fluorescent dye AF488 (Ex. 490 nm, Em. 525 nm) were used. The 6-panel image depicts high background-to-probe signal and inconclusive CTX-AF488 labelling of U87 cells when compared to control. Scale bar, 20 μm.

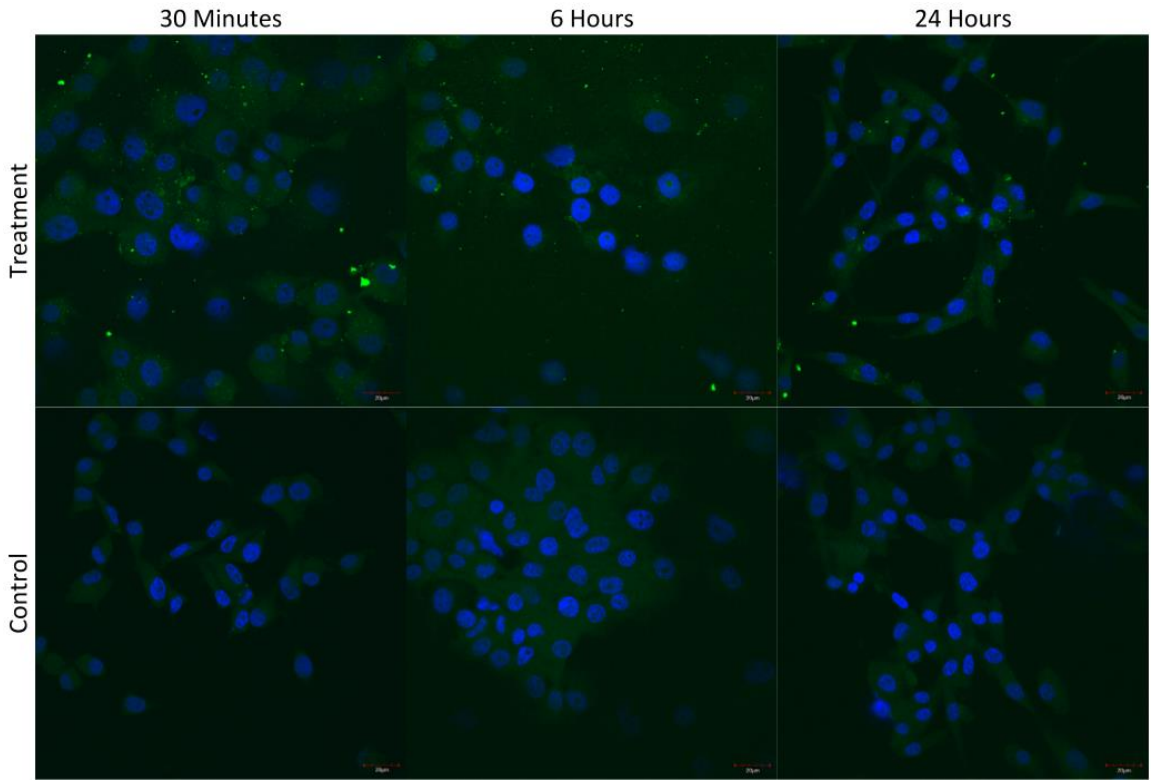

Figure 12. Labelling of U87 Cell Line with rBSG-AF488. Serum-free EMEM media alone (i.e. control) or that containing rBSG-AF488 was used to treat 50,000 CFU U87 GBM cells *in vitro* via 8-well chambered slides for 30 minutes under normoxic conditions. Post-treatment incubation under normoxic ensued for 30 minutes, 6 hours, or 24 hours prior to 4% paraformaldehyde fixation and imaging with confocal microscopy. An Olympus FLUOVIEW FV1000 laser scanning confocal microscope employed a scanning speed of 20 μs/pixel and 800 X 800 aspect ratio to obtain 60x images. The nuclear counterstain DAPI (Ex. 405 nm, Em. 461 nm) and green fluorescent dye AF488 (Ex. 490 nm, Em. 525 nm) were used. The 6-panel image is suggestive of rBSG U87 cell-labelling due to increase signal and number of punctate surrounding U87 nuclei when compared to control. Scale bar, 20 μm.

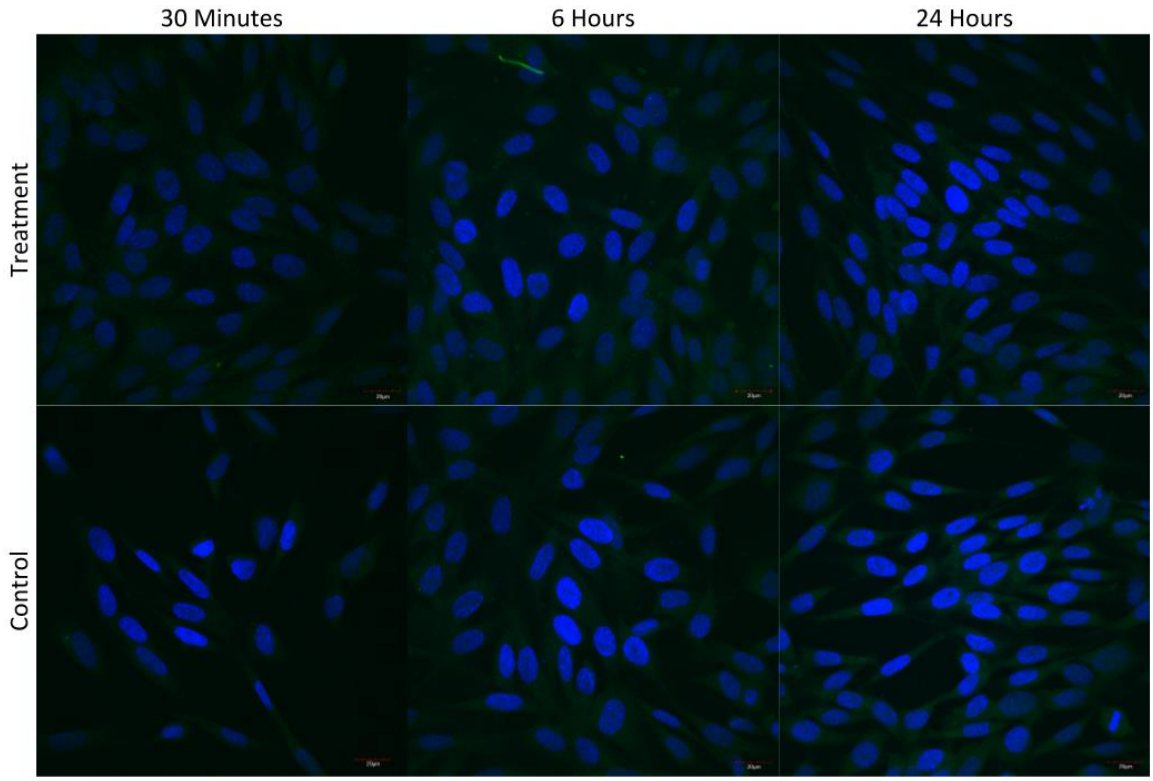

Figure 13. Labelling of MSU1.1 Cell Line with CTX-AF488. Serum-free EMEM media alone (i.e. control) or that containing CTX-AF488 was used to treat 50,000 CFU MSU1.1 foreskin fibroblasts cells *in vitro* via 8-well chambered slides for 30 minutes under normoxic conditions. Post-treatment incubation under normoxic ensued for 30 minutes, 6 hours, or 24 hours prior to 4% paraformaldehyde fixation and imaging with confocal microscopy. An Olympus FLUOVIEW FV1000 laser scanning confocal microscope employed a scanning speed of 20 µs/pixel and 800 X 800 aspect ratio to obtain 60x images. The nuclear counterstain DAPI (Ex. 405 nm, Em. 461 nm) and green fluorescent dye AF488 (Ex. 490 nm, Em. 525 nm) were used. The 6-panel image depicts low background-to-probe signal and unobservable CTX-AF488 labelling of U87 cells when compared to control. Scale bar, 20 µm.

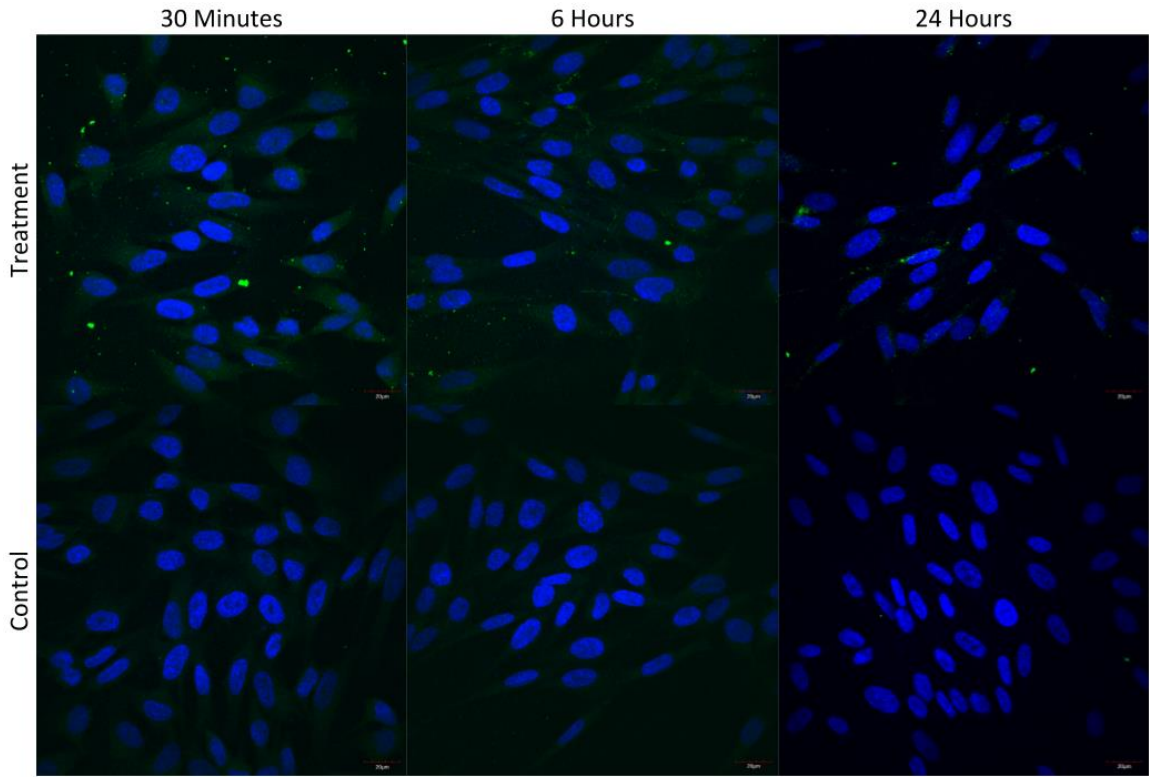

Figure 14. Labelling of MSU1.1 Cell Line with rBSG-AF488. Serum-free EMEM media alone (i.e. control) or that containing rBSG-AF488 was used to treat 50,000 CFU MSU1.1 foreskin fibroblasts cells *in vitro* via 8-well chambered slides for 30 minutes under normoxic conditions. Post-treatment incubation under normoxic ensued for 30 minutes, 6 hours, or 24 hours prior to 4% paraformaldehyde fixation and imaging with confocal microscopy. An Olympus FLUOVIEW FV1000 laser scanning confocal microscope employed a scanning speed of 20 µs/pixel and 800 X 800 aspect ratio to obtain 60x images. The nuclear counterstain DAPI (Ex. 405 nm, Em. 461 nm) and green fluorescent dye AF488 (Ex. 490 nm, Em. 525 nm) were used. The 6-panel image is suggestive of rBSG-AF488 MSU1.1 cell-labelling due to increase signal and punctate number surrounding MSU1.1 nuclei when compared to control. Scale bar, 20 µm.

DISCUSSION

Glioblastoma is a type of high-grade neurological tumor of glial origin. Following standard treatment involving tumor resection, chemotherapy, and radiotherapy, the 5-year survival rate following diagnosis remains at ~ 5%. Obstacles to efficacious treatment include the inherent location of the tumor (within the brain), impermeability of chemotherapy across the BBB, tumor cell population heterogeneity, and rapid metastasis of cells from the diffuse tumor margin which imprecates full-tumor resection. Developing novel therapies requires a change in treatment paradigm. Oncolytic therapy, CAR-T immunotherapy, and immune checkpoint inhibitors (i.e. PD-L1) have showed promise. However, a multivalent treatment option is needed which leverages the pillars of cancer progression.

Glioblastoma utilizes membrane-bound cell surface proteins to facilitate metastasis and tumorigenesis. A new category of biologicals, termed “theranostics” (*thera-*, therapy; *-nostics*, diagnostic indicator), can detect the tumor, serve as a tumor-specific chemotherapeutic, and possess inherent antitumoral activity. Advantages of theranostics are their tumor-specific drug delivery, ability to pass the BBB, low off-target effects on non-cancerous tissue, and ability to detect and monitor tumor progression and resection. This work aimed to characterize the synthesis and efficacy of 2 peptides, one experimental theranostic and one which is currently under FDA review.

Chlorotoxin was the first native small peptide to show *in vitro* (Ullrich et al., 1995) and *in situ* (Soroceanu et al., 1998) tumor-labelling specificity. Since its isolation from Israeli Deathstalker scorpion venom in the 1990s, its specificity for CLC, MMP-2, αvβ3 integrin, and annexin-2 have been established (Veiseh et al., 2007). Consequently, these cell-surface proteins are highly-expressed on GBM tumor cells and fundamental for GBM tumor progression. Prior unpublished work in our lab concluded that fluorescently-labelled canonical 36 amino acid sequence CTX peptide can label HF2303 CSCs and adherent GBM cell lines LN229 and U87. The human foreskin fibroblast cell line MSU 1.1 served as negative control which was not labelled by CTX. To further this previous finding, this work utilized Xu et al.'s 35 amino acid CTX sequence (termed CA4) which was characterized to have a greater anti-angiogenic potential than canonical sequence CTX (2016). A novel nucleic acid sequence coding for CA4 (hereafter referred to as rCTX) was created for a prokaryotic periplasmic expression system to conserve rCTX tertiary structure require for rCTX function (Figure 2). Upon Bsa1-mediated linearization of empty expression plasmid (Figure 3) and donor plasmid containing the rCTX oligo (Figure 4.), ligation of the two products was performed to obtain expression plasmid. Figure 5 illustrates the proposed BsaI digestion and ligation scheme. Sanger sequencing of the expression plasmid revealed that rCTX oligo did ligate into the correct reading frame of the expression plasmid's multiple cloning site (MCS; Figure 6). Following protein induction under optimized conditions (data not shown), purification of protein was attempted by IMAC and the C-terminal 6 residue histidine-tag encoded by the rCTX oligo. Purification of soluble rCTX was unsuccessful due to the absence of anticipated ~ 6.5 kDa product on SDS-PAGE (Figure 7). It is understood that overexpression of

recombinant protein can results in insoluble inclusion bodies. Roughly 70% of recombinant protein express as inclusion bodies (Yang et al., 2011). To detect expression of insoluble rCTX, various denaturation and precipitation schemes to yield insoluble protein prior to purification were attempted. A two-step denaturation process was initially attempted (Figure 8) as previously described by Yang et al. (2011). The lack of ~ 6.5 kDa banding in any of the SDS-PAGE lanes indicated that soluble and insoluble-expressed rCTX were absent; IMAC purification was not performed. Following this result, a one-step solubalization scheme was performed. As performed by Dai et al., purification of insoluble small-peptides like disulfide bond-rich venom proteins can be achieved by a one-step denaturation and solubilization process (2012). Induced rCTX lysate was exposed to the strong chaotropic agent for either 30 minutes (Figure 9) or 16 hours (Figure 10) prior to renaturation and batch purification of putative rCTX. No ~ 6.5 kDa banding was present in any lane from either of the two attempts which suggests that rCTX is not expressed in an insoluble form. To summarize, this data supports the conclusion that recombinant protein purification of a small venom peptide such as rCTX via a 6-histidine N-terminal tag is problematic. However, one observation which is consistent among all rCTX induction and purification SDS-PAGE images are the whole-lane densitometry scores relative to uninduced cell lysates. Induced lysates show overall lower levels endogenous protein expression when compared to plasmid-transformed uninduced bacterial lysates. This suggests that rCTX may be produced and quickly degraded or recycled by the *E. coli.* This hypothesis is supported in that *E. coli* have membrane-localized chloride-ion channels (CIC) homologous to human CICs (Jentsch et al., 2002; Koprowski & Kubalski, 2001). Upon expression of rCTX, its interaction with

endogenous bacterial CICs may induce its immediate degradation and subsequent detection of recombinant protein by SDS-PAGE. Previous groups have successfully-produced CTX via bacterial expression system with purification via glutathione tag (Xu et al., 2016). In comparison to the 6 amino acid histidine tag purification system used here, glutathione is a 25 kDa tag which is significantly larger and possibly able to sterically hinder expressed rCTX from binding to CICs which is followed by degradation. The histidine tag purification method was used here in attempt to eliminate the tag-cleavage step from recombinant peptide which is required following purification.

In stark contracts to rCTX purification efforts, purification of rBSG in accordance with Belton et.al (2008) was successful (Figure 1). The same purification scheme was used for both peptides. rBSG was present in all lysate, IMAC wash, and elution fractions following purification (Figure 1). Thus, purified rBSG was used to *in vitro* cell labelling assay following desalting and depyrogenation of peptide via multiple centrifugal washes.

rBSG was included in this study due to its interaction with membrane-bound proteins which are overexpressed in GBM or crucial for tumorigenesis. Such interaction partners are basigin-2, CD44, various MMPs including MMP-2, EGFR, cyclophilin 60, and MT1-MMP, and caveolin-1 (Belton et. al., 20008; Reviewed by Grass et al., 2014; Biswas et al., 1995; Grass et al., 2012; Pushkarsky et al., 2005; Tang et al., 2004). As with CTX, soluble basigin can cross the BBB and its various interaction partners are generally attributed with tumorigenesis which suggests that rBSG could also be used as a theranostic. *In vitro* cell labelling assay with U87 GBM cell line or MSU 1.1 human

foreskin fibroblast control cell line were subjected to 5 μM (i.e. 116 μg/mL) treatment of fluorescently-conjugated purified rBSG or commercially-obtained CTX (5 μM; 20.8 μg/mL) for 30 minutes at 37 °C. A 5 μM treatment concentration was used for both peptides to qualitatively determine which of the two peptides labelled cells with greater efficacy. These treatment concentrations and times were used due to previous finding by Belton et. al where it was concluded that an *in vitro* treatment of 50 μg/ml rBSG for 10 minutes at 37 °C could successfully labels uterine fibroblasts (2008). Fixation with 4% PFA and mounting of cell culture slides with DAPI-containing mountant was performed prior to confocal microscopy. Treatment of U87 cells with fluorescent CTX or rBSG produced variable results. U87 cells treated with CTX-AF488 resulted in a high background-to-probe signal when comparing treatment to control images, regardless of time point (Figure 11). Cellular autofluorescence is depicted in control images. This may be due to the high gain setting during image acquisition which was needed to detect CTX-AF488 signal. Based on this result, the data suggests that CTX does not label U87 GBM cells *in vitro*, but previous literature does not corroborate with this finding (Veiseh et al., 2007; Wiranowska et al., 2011; Xu et al., 2016). Analysis of rBSG-AF488 treated U87 cells depicts strong signal which overlaps with DAPI signal when compared to controls (Figure 12). Also present in treatment images are punctate which seem to be localized to cell bodies. An explanation of this phenomenon may be due to soluble rBSG homodimerization when in solution (Belton et.al, 2008). This phenomenon may not be preventable as dimerization is an innate property of rBSG-2. In obtaining MSU1.1 human foreskin fibroblast cell images following treatment with CTX-AF488, no signal was observed, regardless of time point, when compared to control images (Figure 13). This

result was expected as other works have observed similar findings (Lyons et al., 2002). Although background-to-probe signal was low, it should be noted the CTX-AF488 did not label U87 cells, and this was expected. MSU1.1 cells when treated with rBSG-AF488 did exhibit positive labelling, low background-to-noise signal, and loss of signal over time when compared to non-treated controls (Figure 14). It is well established that rBSG can binds to fibroblasts due to their cell surface expression of basigin-2 and role in extracellular remodeling *in vivo* (Belton et al., 2008). This result does not support rBSG for use as a cancer theranostic as non-cancerous tissue would be labeled during treatment. Although basigin is expressed within the CNS of mice (Fan et al., 1998) and presumably in that of humans, basigin's use as a theranostic for GBM treatment may outweigh any foreseeable complications. This aside, characterizing rBSG's specificity for other pathological tissues such as those which bind CTX would be of benefit. Also, further work in determining rBSG receptors on GBM cells should be the first step in directing or engineering rBSG to be specific for GBM tissue.

CONCLUSION

Glioblastoma is an aggressive neurological disease for which the standard of care including adjuvant chemotherapy, surgery, and radiotherapy does little in increasing the 5-year overall patient survival of 5.1% (Ostrom et al., 2015). This study aimed to characterize a new class of small-peptide therapeutic which has vehicle, inherent antitumor activity, and cell visualization ability (termed *theranostic*). Two such theranostics studied in this work include the 4 kDa peptide chlorotoxin (CTX) and the 25 kDa sized extracellular domain portion of basigin-2 (rBSG). The working hypothesis of this study was supported by observing differential labelling ability of both peptides on U87 GBM and MSU1.1 human foreskin fibroblast cell lines, as determined by *in vitro* assay and confocal microscopy. In pursuing this work, a novel cDNA sequence coding for a variant of CTX peptide (termed rCTX) was produced and properly ligated into vector for a periplasmic bacterial expression and histidine tag purification. However, it was concluded that histidine tag purification of CTX is not obtainable. The hypothesis supporting this result is based on the small 6 amino acid histidine tag. The tag's inability to provide steric hindrance and interaction inhibition of CTX with bacterial chloride ion channels facilitates CTX's degradation following expression. Considering these findings, rBSG and CTX are still viable treatment options for GBM and possibly other pathologies due to their multivalent ability in disease treatment.

REFERENCES

Agrawal, S. M., & Yong, V. W. (2011). The many faces of EMMPRIN—Roles in neuroinflammation. *Biochimica et Biophysica Acta (BBA) - Molecular Basis of Disease*, *1812*(2), 213–219. https://doi.org/10.1016/j.bbadis.2010.07.018

Banerjee, A., Lee, A., Campbell, E., & MacKinnon, R. (2013). Structure of a pore-blocking toxin in complex with a eukaryotic voltage-dependent K+ channel. *ELife*, *2*. https://doi.org/10.7554/eLife.00594

Bauer, G. A., & Burgers, P. M. (1988). The yeast analog of mammalian cyclin/proliferating-cell nuclear antigen interacts with mammalian DNA polymerase delta. *Proceedings of the National Academy of Sciences of the United States of America*, *85*(20), 7506–7510.

Bauvois, B. (2012). New facets of matrix metalloproteinases MMP-2 and MMP-9 as cell surface transducers: Outside-in signaling and relationship to tumor progression. *Biochimica et Biophysica Acta (BBA) - Reviews on Cancer*, *1825*(1), 29–36. https://doi.org/10.1016/j.bbcan.2011.10.001

Belton, R. J., Chen, L., Mesquita, F. S., & Nowak, R. A. (2008). Basigin-2 is a cell surface receptor for soluble basigin ligand. *The Journal of Biological Chemistry*, *283*(26), 17805–17814. https://doi.org/10.1074/jbc.M801876200

Bigner, D. D. (2011, December 1). PVSRIPO for Recurrent Glioblastoma (GBM). Retrieved May 8, 2016, from https://clinicaltrials.gov/ct2/show/study/NCT01491893

Biswas, C. (1984). Collagenase stimulation in cocultures of human fibroblasts and human tumor cells. *Cancer Letters*, *24*(2), 201–207.

Biswas, C., Zhang, Y., DeCastro, R., Guo, H., Nakamura, T., Kataoka, H., & Nabeshima, K. (1995). The human tumor cell-derived collagenase stimulatory factor (renamed EMMPRIN) is a member of the immunoglobulin superfamily. *Cancer Research*, *55*(2), 434–439.

Björklund, M., & Koivunen, E. (2005). Gelatinase-mediated migration and invasion of cancer cells. *Biochimica Et Biophysica Acta*, *1755*(1), 37–69. https://doi.org/10.1016/j.bbcan.2005.03.001

Bontems, F., Roumestand, C., Gilquin, B., Ménez, A., & Toma, F. (1991). Refined structure of charybdotoxin: common motifs in scorpion toxins and insect defensins. *Science (New York, N.Y.)*, *254*(5037), 1521–1523.

Bruno, S., & Darzynkiewicz, Z. (1992). Cell cycle dependent expression and stability of the nuclear protein detected by Ki-67 antibody in HL-60 cells. *Cell Proliferation*, *25*(1), 31–40. https://doi.org/10.1111/j.1365-2184.1992.tb01435.x

Calabrese, C., Poppleton, H., Kocak, M., Hogg, T. L., Fuller, C., Hamner, B., … Gilbertson, R. J. (2007). A Perivascular Niche for Brain Tumor Stem Cells. *Cancer Cell*, *11*(1), 69–82. https://doi.org/10.1016/j.ccr.2006.11.020

Camenisch, T. D., Spicer, A. P., Brehm-Gibson, T., Biesterfeldt, J., Augustine, M. L., Calabro, A., … McDonald, J. A. (2000). Disruption of hyaluronan synthase-2 abrogates normal cardiac morphogenesis and hyaluronan-mediated transformation of epithelium to mesenchyme. *The Journal of Clinical Investigation*, *106*(3), 349–360. https://doi.org/10.1172/JCI10272

Chan-Ling, T., McLeod, D. S., Hughes, S., Baxter, L., Chu, Y., Hasegawa, T., & Lutty, G. A. (2004). Astrocyte-endothelial cell relationships during human retinal vascular development. *Investigative Ophthalmology & Visual Science*, *45*(6), 2020–2032.

Chetty, C., Lakka, S. S., Bhoopathi, P., & Rao, J. S. (2010). MMP-2 alters VEGF expression via alphaVbeta3 integrin-mediated PI3K/AKT signaling in A549 lung cancer cells. *International Journal of Cancer*, *127*(5), 1081–1095. https://doi.org/10.1002/ijc.25134

Corbeil, D., Röper, K., Hellwig, A., Tavian, M., Miraglia, S., Watt, S. M., … Huttner, W. B. (2000). The human AC133 hematopoietic stem cell antigen is also expressed in epithelial cells and targeted to plasma membrane protrusions. *The Journal of Biological Chemistry*, *275*(8), 5512–5520.

Craik, D. J., Daly, N. L., & Waine, C. (2001). The cystine knot motif in toxins and implications for drug design. *Toxicon*, *39*(1), 43–60. https://doi.org/10.1016/S0041-0101(00)00160-4

Dai, H., Yin, S., Li, T., Cao, Z., Ji, Y., Wu, Y., & Li, W. (2012). Recombinant expression, purification, and characterization of scorpion toxin BmαTX14. *Protein Expression and Purification*, *82*(2), 325–331. https://doi.org/10.1016/j.pep.2012.02.001

Dai, J., Dou, K., Wang, C., Zhao, P., Lau, W. B., Tao, L., … Chen, Z. (2009). The interaction of HAb18G/CD147 with integrin alpha6beta1 and its implications for the invasion potential of human hepatoma cells. *BMC Cancer*, *9*, 337. https://doi.org/10.1186/1471-2407-9-337

Dai, L., Guinea, M. C., Slomiany, M. G., Bratoeva, M., Grass, G. D., Tolliver, L. B., … Toole, B. P. (2013). CD147-dependent heterogeneity in malignant and chemoresistant properties of cancer cells. *The American Journal of Pathology*, *182*(2), 577–585. https://doi.org/10.1016/j.ajpath.2012.10.011

Darzynkiewicz, Z., Zhao, H., Zhang, S., Lee, M. Y. W. T., Lee, E. Y. C., & Zhang, Z. (2015). Initiation and termination of DNA replication during S phase in relation to cyclins D1, E and A, p21WAF1, Cdt1 and the p12 subunit of DNA polymerase δ revealed in individual cells by cytometry. *Oncotarget*, *6*(14), 11735–11750. https://doi.org/10.18632/oncotarget.4149

DeBin, J. A., Maggio, J. E., & Strichartz, G. R. (1993). Purification and characterization of chlorotoxin, a chloride channel ligand from the venom of the scorpion. *The American Journal of Physiology*, *264*(2 Pt 1), C361-369.

Dennis, J. W., Granovsky, M., & Warren, C. E. (1999). Glycoprotein glycosylation and cancer progression. *Biochimica Et Biophysica Acta*, *1473*(1), 21–34.

Eckel-Passow, J. E., Lachance, D. H., Molinaro, A. M., Walsh, K. M., Decker, P. A., Sicotte, H., … Jenkins, R. B. (2015). Glioma Groups Based on 1p/19q, IDH, and TERT Promoter Mutations in Tumors. *New England Journal of Medicine*, *372*(26), 2499–2508. https://doi.org/10.1056/NEJMoa1407279

El-Ghlban, S., Kasai, T., Shigehiro, T., Yin, H. X., Sekhar, S., Ida, M., … Seno, M. (2014). Chlorotoxin-Fc Fusion Inhibits Release of MMP-2 from Pancreatic Cancer Cells, Chlorotoxin-Fc Fusion Inhibits Release of MMP-2 from Pancreatic Cancer Cells. *BioMed Research International*, *BioMed Research International*, *2014*, *2014*, e152659. https://doi.org/10.1155/2014/152659, 10.1155/2014/152659

Emami, S., & Dadashpour, S. (2015). Current developments of coumarin-based anti-cancer agents in medicinal chemistry. *European Journal of Medicinal Chemistry*, *102*, 611–630. https://doi.org/10.1016/j.ejmech.2015.08.033

Esteller, M., Garcia-Foncillas, J., Andion, E., Goodman, S. N., Hidalgo, O. F., Vanaclocha, V., … Herman, J. G. (2000). Inactivation of the DNA-Repair Gene *MGMT* and the Clinical Response of Gliomas to Alkylating Agents. *New England Journal of Medicine*, *343*(19), 1350–1354. https://doi.org/10.1056/NEJM200011093431901

Evans, S. M., Judy, K. D., Dunphy, I., Jenkins, W. T., Nelson, P. T., Collins, R., … Koch, C. J. (2004). Comparative Measurements of Hypoxia in Human Brain Tumors Using Needle Electrodes and EF5 Binding. *Cancer Research*, *64*(5), 1886–1892. https://doi.org/10.1158/0008-5472.CAN-03-2424

Fadool, J. M., & Linser, P. J. (1993). 5A11 antigen is a cell recognition molecule which is involved in neuronal-glial interactions in avian neural retina. *Developmental Dynamics: An Official Publication of the American Association of Anatomists*, *196*(4), 252–262. https://doi.org/10.1002/aja.1001960406

Fan, Q.-W., Yuasa, S., Kuno, N., Senda, T., Kobayashi, M., Muramatsu, T., & Kadomatsu, K. (1998). Expression of basigin, a member of the immunoglobulin superfamily, in the mouse central nervous system. *Neuroscience Research*, *30*(1), 53–63. https://doi.org/10.1016/S0168-0102(97)00119-3

Friedman, H. S., Prados, M. D., Wen, P. Y., Mikkelsen, T., Schiff, D., Abrey, L. E., … Cloughesy, T. (2009). Bevacizumab Alone and in Combination With Irinotecan in Recurrent Glioblastoma. *Journal of Clinical Oncology*, *27*(28), 4733–4740. https://doi.org/10.1200/JCO.2008.19.8721

Fu, Y., Zheng, S., Zheng, Y., Huang, R., An, N., Liang, A., & Hu, C. (2012). Glioma derived isocitrate dehydrogenase-2 mutations induced up-regulation of HIF-1α and β-catenin signaling: Possible impact on glioma cell metastasis and chemo-resistance. *The International Journal of Biochemistry & Cell Biology*, *44*(5), 770–775. https://doi.org/10.1016/j.biocel.2012.01.017

Gerke, V., Creutz, C. E., & Moss, S. E. (2005). Annexins: linking Ca2+ signalling to membrane dynamics. *Nature Reviews. Molecular Cell Biology*, *6*(6), 449–461. https://doi.org/10.1038/nrm1661

Gerke, V., & Moss, S. E. (2002). Annexins: from structure to function. *Physiological Reviews*, *82*(2), 331–371. https://doi.org/10.1152/physrev.00030.2001

Ghatak, S., Misra, S., & Toole, B. P. (2005). Hyaluronan Constitutively Regulates ErbB2 Phosphorylation and Signaling Complex Formation in Carcinoma Cells. *Journal of Biological Chemistry*, *280*(10), 8875–8883. https://doi.org/10.1074/jbc.M410882200

Giancotti, F. G., & Ruoslahti, E. (1999). Integrin signaling. *Science (New York, N.Y.)*, *285*(5430), 1028–1032.

Goetz, C., & Gromeier, M. (2010). Preparing an Oncolytic Poliovirus Reombinant for Clinical Application Against Glioblastoma Multiforme. *Cytokine & Growth Factor Reviews*, *21*(2–3), 197–203. https://doi.org/10.1016/j.cytogfr.2010.02.005

Gonzalez-Perez, O., & Alvarez-Buylla, A. (2011). Oligodendrogenesis in the subventricular zone and the role of epidermal growth factor. *Brain Research Reviews*, *67*(1–2), 147–156. https://doi.org/10.1016/j.brainresrev.2011.01.001

Gonzalez-Perez, O., Jauregui-Huerta, F., & Galvez-Contreras, A. Y. (2010). Immune system modulates the function of adult neural stem cells. *Current Immunology Reviews*, *6*(3), 167–173. https://doi.org/10.2174/157339510791823772

Goodman, S. L., Hölzemann, G., Sulyok, G. A. G., & Kessler, H. (2002). Nanomolar small molecule inhibitors for alphav(beta)6, alphav(beta)5, and alphav(beta)3 integrins. *Journal of Medicinal Chemistry*, *45*(5), 1045–1051.

Grass, G. D., Bratoeva, M., & Toole, B. P. (2012). Regulation of invadopodia formation and activity by CD147. *Journal of Cell Science*, *125*(Pt 3), 777–788. https://doi.org/10.1242/jcs.097956

Grass, G. D., Dai, L., Qin, Z., Parsons, C., & Toole, B. P. (2014). CD147: regulator of hyaluronan signaling in invasiveness and chemoresistance. *Advances in Cancer Research*, *123*, 351–373. https://doi.org/10.1016/B978-0-12-800092-2.00013-7

Guo, H., Majmudar, G., Jensen, T. C., Biswas, C., Toole, B. P., & Gordon, M. K. (1998). Characterization of the gene for human EMMPRIN, a tumor cell surface inducer of matrix metalloproteinases. *Gene*, *220*(1–2), 99–108.

Hanahan, D., & Weinberg, R. A. (2000). The hallmarks of cancer. *Cell*, *100*(1), 57–70.

Hanna, S. M., Kirk, P., Holt, O. J., Puklavec, M. J., Brown, M. H., & Barclay, A. N. (2003). A novel form of the membrane protein CD147 that contains an extra Ig-like domain and interacts homophilically. *BMC Biochemistry*, *4*, 17. https://doi.org/10.1186/1471-2091-4-17

Hegi, M. E., Diserens, A.-C., Gorlia, T., Hamou, M.-F., de Tribolet, N., Weller, M., … Stupp, R. (2005). MGMT Gene Silencing and Benefit from Temozolomide in Glioblastoma. *New England Journal of Medicine*, *352*(10), 997–1003. https://doi.org/10.1056/NEJMoa043331

Hernandez-Barrantes, S., Toth, M., Bernardo, M. M., Yurkova, M., Gervasi, D. C., Raz, Y., … Fridman, R. (2000). Binding of active (57 kDa) membrane type 1-matrix metalloproteinase (MT1-MMP) to tissue inhibitor of metalloproteinase (TIMP)-2 regulates MT1-MMP processing and pro-MMP-2 activation. *The Journal of Biological Chemistry*, *275*(16), 12080–12089.

Horn, P. A., Tesch, H., Staib, P., Kube, D., Diehl, V., & Voliotis, D. (1999). Expression of AC133, a novel hematopoietic precursor antigen, on acute myeloid leukemia cells. *Blood*, *93*(4), 1435–1437.

Hoshino, T., Nagashima, T., Murovic, J., Levin, E. M., Levin, V. A., & Rupp, S. M. (1985). Cell kinetic studies of in situ human brain tumors with bromodeoxyuridine. *Cytometry*, *6*(6), 627–632. https://doi.org/10.1002/cyto.990060619

Ihrie, R. A., & Álvarez-Buylla, A. (2011). Lake-Front Property: A Unique Germinal Niche by the Lateral Ventricles of the Adult Brain. *Neuron*, *70*(4), 674–686. https://doi.org/10.1016/j.neuron.2011.05.004

J. Deshane, C.C. Garner, & H. Sontheimer. (2002). Chlorotoxin Inhibits Glioma Cell Invasion via Matrix Metalloproteinase-2. *Journal of Biological Chemistry*, *278*(6), 4135–4144. https://doi.org/10.1074/jbc.M205662200

Jeffrey N Bruce, MD, Jules E Harris, MD, & Benjamin Kennedy, MD. (2015). Glioblastoma Multiforme Treatment & Management: Medical Care, Surgical Care, Consultations. Retrieved from http://emedicine.medscape.com/article/283252-treatment

Jentsch, T. J., Stein, V., Weinreich, F., & Zdebik, A. A. (2002). Molecular Structure and Physiological Function of Chloride Channels. *Physiological Reviews*, *82*(2), 503–568. https://doi.org/10.1152/physrev.00029.2001

Jiang, A., Lehti, K., Wang, X., Weiss, S. J., Keski-Oja, J., & Pei, D. (2001). Regulation of membrane-type matrix metalloproteinase 1 activity by dynamin-mediated endocytosis. *Proceedings of the National Academy of Sciences of the United States of America*, *98*(24), 13693–13698. https://doi.org/10.1073/pnas.241293698

Kalkan, R. (2015). Glioblastoma Stem Cells as a New Therapeutic Target for Glioblastoma. *Clinical Medicine Insights. Oncology*, *9*, 95–103. https://doi.org/10.4137/CMO.S30271

Kalluri, R., & Weinberg, R. A. (2009). The basics of epithelial-mesenchymal transition. *The Journal of Clinical Investigation*, *119*(6), 1420–1428. https://doi.org/10.1172/JCI39104

Kaname, T., Miyauchi, T., Kuwano, A., Matsuda, Y., Muramatsu, T., & Kajii, T. (1993). Mapping basigin (BSG), a member of the immunoglobulin superfamily, to 19p13.3. *Cytogenetics and Cell Genetics*, *64*(3–4), 195–197. https://doi.org/10.1159/000133573

Kesavan, K., Ratliff, J., Johnson, E. W., Dahlberg, W., Asara, J. M., Misra, P., … Jacoby, D. B. (2010). Annexin A2 Is a Molecular Target for TM601, a Peptide with Tumor-targeting and Anti-angiogenic Effects. *The Journal of Biological Chemistry*, *285*(7), 4366–4374. https://doi.org/10.1074/jbc.M109.066092

Killela, P. J., Reitman, Z. J., Jiao, Y., Bettegowda, C., Agrawal, N., Diaz, L. A., … Yan, H. (2013). TERT promoter mutations occur frequently in gliomas and a subset of tumors derived from cells with low rates of self-renewal. *Proceedings of the National Academy of Sciences of the United States of America*, *110*(15), 6021–6026. https://doi.org/10.1073/pnas.1303607110

Kong, L.-M., Liao, C.-G., Chen, L., Yang, H.-S., Zhang, S.-H., Zhang, Z., … Chen, Z.-N. (2011). Promoter hypomethylation up-regulates CD147 expression through increasing Sp1 binding and associates with poor prognosis in human hepatocellular carcinoma. *Journal of Cellular and Molecular Medicine*, *15*(6), 1415–1428. https://doi.org/10.1111/j.1582-4934.2010.01124.x

Koprowski, P., & Kubalski, A. (2001). Bacterial ion channels and their eukaryotic homologues. *BioEssays*, *23*(12), 1148–1158. https://doi.org/10.1002/bies.10017

Kuzmenkov, A. I., Grishin, E. V., & Vassilevski, A. A. (2015). Diversity of Potassium Channel Ligands: Focus on Scorpion Toxins. *Biochemistry. Biokhimiia*, *80*(13), 1764–1799. https://doi.org/10.1134/S0006297915130118

Kuzmenkov, Alexey I., Krylov, N. A., Chugunov, A. O., Grishin, E. V., & Vassilevski, A. A. (2016). Kalium: a database of potassium channel toxins from scorpion venom. *Database: The Journal of Biological Databases and Curation*, *2016*. https://doi.org/10.1093/database/baw056

Li, Y., Wu, J., Song, F., Tang, J., Wang, S.-J., Yu, X.-L., … Jiang, J.-L. (2012). Extracellular membrane-proximal domain of HAb18G/CD147 binds to metal ion-dependent adhesion site (MIDAS) motif of integrin β1 to modulate malignant properties of hepatoma cells. *The Journal of Biological Chemistry*, *287*(7), 4759–4772. https://doi.org/10.1074/jbc.M111.277699

Liang, L., Major, T., & Bocan, T. (2002). Characterization of the promoter of human extracellular matrix metalloproteinase inducer (EMMPRIN). *Gene*, *282*(1–2), 75–86.

Liao, C.-G., Kong, L.-M., Song, F., Xing, J.-L., Wang, L.-X., Sun, Z.-J., … Chen, Z.-N. (2011). Characterization of Basigin Isoforms and the Inhibitory Function of Basigin-3 in Human Hepatocellular Carcinoma Proliferation and Invasion. *Molecular and Cellular Biology*, *31*(13), 2591–2604. https://doi.org/10.1128/MCB.05160-11

Lipkind, G. M., & Fozzard, H. A. (1997). A model of scorpion toxin binding to voltage-gated K+ channels. *The Journal of Membrane Biology*, *158*(3), 187–196.

Lippens, G., Najib, J., Wodak, S. J., & Tartar, A. (1995). NMR sequential assignments and solution structure of chlorotoxin, a small scorpion toxin that blocks chloride channels. *Biochemistry*, *34*(1), 13–21.

Lyons, S. A., O'Neal, J., & Sontheimer, H. (2002). Chlorotoxin, a scorpion-derived peptide, specifically binds to gliomas and tumors of neuroectodermal origin. *Glia*, *39*(2), 162–173. https://doi.org/10.1002/glia.10083

Madureira, P. A., Hill, R., Miller, V. A., Giacomantonio, C., Lee, P. W., & Waisman, D. M. (2011). Annexin A2 is a novel Cellular Redox Regulatory Protein involved in Tumorigenesis. *Oncotarget*, *2*(12), 1075–1093. https://doi.org/10.18632/oncotarget.375

Manoharan, C., Wilson, M. C., Sessions, R. B., & Halestrap, A. P. (2006). The role of charged residues in the transmembrane helices of monocarboxylate transporter 1 and its ancillary protein basigin in determining plasma membrane expression and catalytic activity. *Molecular Membrane Biology*, *23*(6), 486–498. https://doi.org/10.1080/09687860600841967

Marieb, E. A., Zoltan-Jones, A., Li, R., Misra, S., Ghatak, S., Cao, J., … Toole, B. P. (2004). Emmprin Promotes Anchorage-Independent Growth in Human Mammary Carcinoma Cells by Stimulating Hyaluronan Production. *Cancer Research*, *64*(4), 1229–1232. https://doi.org/10.1158/0008-5472.CAN-03-2832

Martuza, R., Malick, A., Markert, J., Ruffner, K., & Coen, D. (1991). Experimental therapy of human glioma by means of a genetically engineered virus mutant. *Science*, *252*(5007), 854–856. https://doi.org/10.1126/science.1851332

Meng, W., & Takeichi, M. (2009). Adherens Junction: Molecular Architecture and Regulation. *Cold Spring Harbor Perspectives in Biology*, *1*(6). https://doi.org/10.1101/cshperspect.a002899

Merrill, M. K., Bernhardt, G., Sampson, J. H., Wikstrand, C. J., Bigner, D. D., & Gromeier, M. (2004). Poliovirus receptor CD155-targeted oncolysis of glioma. *Neuro-Oncology*, *6*(3), 208–217. https://doi.org/10.1215/S1152851703000577

Misra, S., Ghatak, S., & Toole, B. P. (2005). Regulation of MDR1 Expression and Drug Resistance by a Positive Feedback Loop Involving Hyaluronan, Phosphoinositide 3-Kinase, and ErbB2. *Journal of Biological Chemistry*, *280*(21), 20310–20315. https://doi.org/10.1074/jbc.M500737200

Miyauchi, T., Kanekura, T., Yamaoka, A., Ozawa, M., Miyazawa, S., & Muramatsu, T. (1990). Basigin, a new, broadly distributed member of the immunoglobulin superfamily, has strong homology with both the immunoglobulin V domain and the beta-chain of major histocompatibility complex class II antigen. *Journal of Biochemistry*, *107*(2), 316–323.

Mizrak, D., Brittan, M., & Alison, M. R. (2008). CD133: molecule of the moment. *The Journal of Pathology*, *214*(1), 3–9. https://doi.org/10.1002/path.2283

Montano, N., Cenci, T., Martini, M., D'Alessandris, Q. G., Pelacchi, F., Ricci-Vitiani, L., … Pallini, R. (2011). Expression of EGFRvIII in glioblastoma: prognostic significance revisited. *Neoplasia (New York, N.Y.)*, *13*(12), 1113–1121.

Morgan, T. L., Yang, D. J., Fry, D. G., Hurlin, P. J., Kohler, S. K., Maher, V. M., & McCormick, J. J. (1991). Characteristics of an infinite life span diploid human fibroblast cell strain and a near-diploid strain arising from a clone of cells expressing a transfected v-myc oncogene. *Experimental Cell Research*, *197*(1), 125–136.

Murai, T., Maruyama, Y., Mio, K., Nishiyama, H., Suga, M., & Sato, C. (2011). Low cholesterol triggers membrane microdomain-dependent CD44 shedding and suppresses tumor cell migration. *The Journal of Biological Chemistry*, *286*(3), 1999–2007. https://doi.org/10.1074/jbc.M110.184010

Nooh, H. Z., & Nour-Eldien, N. M. (2016). The dual anti-inflammatory and antioxidant activities of natural honey promote cell proliferation and neural regeneration in a rat model of colitis. *Acta Histochemica*, *118*(6), 588–595. https://doi.org/10.1016/j.acthis.2016.06.006

Nutt, C. L., Mani, D. R., Betensky, R. A., Tamayo, P., Cairncross, J. G., Ladd, C., … Louis, D. N. (2003). Gene Expression-based Classification of Malignant Gliomas Correlates Better with Survival than Histological Classification. *Cancer Research*, *63*(7), 1602–1607.

Ochrietor, J. D., & Linser, P. J. (2004). 5A11/Basigin gene products are necessary for proper maturation and function of the retina. *Developmental Neuroscience*, *26*(5–6), 380–387. https://doi.org/10.1159/000082280

Ochs, K., & Kaina, B. (2000). Apoptosis induced by DNA damage O6-methylguanine is Bcl-2 and caspase-9/3 regulated and Fas/caspase-8 independent. *Cancer Research*, *60*(20), 5815–5824.

Ojeda, P. G., Wang, C. K., & Craik, D. J. (2016). Chlorotoxin: Structure, activity, and potential uses in cancer therapy. *Peptide Science*, *106*(1), 25–36. https://doi.org/10.1002/bip.22748

Oliferenko, S., Paiha, K., Harder, T., Gerke, V., Schwärzler, C., Schwarz, H., … Huber, L. A. (1999). Analysis of CD44-containing lipid rafts: Recruitment of annexin II and stabilization by the actin cytoskeleton. *The Journal of Cell Biology*, *146*(4), 843–854.

Oliveira-Ferrer, L., Hauschild, J., Fiedler, W., Bokemeyer, C., Nippgen, J., Celik, I., & Schuch, G. (2008). Cilengitide induces cellular detachment and apoptosis in endothelial and glioma cells mediated by inhibition of FAK/src/AKT pathway. *Journal of Experimental & Clinical Cancer Research: CR*, *27*, 86. https://doi.org/10.1186/1756-9966-27-86

Ostrom, Q. T., Gittleman, H., Fulop, J., Liu, M., Blanda, R., Kromer, C., … Barnholtz-Sloan, J. S. (2015). CBTRUS Statistical Report: Primary Brain and Central Nervous System Tumors Diagnosed in the United States in 2008-2012. *Neuro-Oncology*, *17*(suppl 4), iv1–iv62. https://doi.org/10.1093/neuonc/nov189

Pakula, R., Melchior, A., Denys, A., Vanpouille, C., Mazurier, J., & Allain, F. (2007). Syndecan-1/CD147 association is essential for cyclophilin B-induced activation of p44/42 mitogen-activated protein kinases and promotion of cell adhesion and chemotaxis. *Glycobiology*, *17*(5), 492–503. https://doi.org/10.1093/glycob/cwm009

Persano, L., Rampazzo, E., Basso, G., & Viola, G. (2013). Glioblastoma cancer stem cells: Role of the microenvironment and therapeutic targeting. *Biochemical Pharmacology*, *85*(5), 612–622. https://doi.org/10.1016/j.bcp.2012.10.001

Pituch-Noworolska, A., Drabik, G., Szatanek, R., Białas, M., Kołodziejczyk, P., Szczepanik, A., … Zembala, M. (2007). Immunophenotype of isolated tumour cells in the blood, bone marrow and lymph nodes of patients with gastric cancer. *Polish Journal of Pathology: Official Journal of the Polish Society of Pathologists*, *58*(2), 93–97.

Pollard, P. J., & Ratcliffe, P. J. (2009). CANCER: Puzzling Patterns of Predisposition. *Science*, *324*(5924), 192–194. https://doi.org/10.1126/science.1173362

Pushkarsky, T., Yurchenko, V., Vanpouille, C., Brichacek, B., Vaisman, I., Hatakeyama, S., … Bukrinsky, M. I. (2005). Cell surface expression of CD147/EMMPRIN is regulated by cyclophilin 60. *The Journal of Biological Chemistry*, *280*(30), 27866–27871. https://doi.org/10.1074/jbc.M503770200

Reardon, D. A., Fink, K. L., Mikkelsen, T., Cloughesy, T. F., O'Neill, A., Plotkin, S., … Nabors, L. B. (2008). Randomized phase II study of cilengitide, an integrin-targeting arginine-glycine-aspartic acid peptide, in recurrent glioblastoma multiforme. *Journal of Clinical Oncology: Official Journal of the American Society of Clinical Oncology*, *26*(34), 5610–5617. https://doi.org/10.1200/JCO.2008.16.7510

Rick, K., Sroka, R., Stepp, H., Kriegmair, M., Huber, R. M., Jacob, K., & Baumgartner, R. (1997). Pharmacokinetics of 5-aminolevulinic acid-induced protoporphyrin IX in skin and blood. *Journal of Photochemistry and Photobiology B: Biology*, *40*(3), 313–319. https://doi.org/10.1016/S1011-1344(97)00076-6

Rupp, P. A., Visconti, R. P., Czirók, A., Cheresh, D. A., & Little, C. D. (2008). Matrix Metalloproteinase 2-Integrin αvβ3 Binding Is Required for Mesenchymal Cell Invasive Activity but Not Epithelial Locomotion: A Computational Time-Lapse Study. *Molecular Biology of the Cell*, *19*(12), 5529–5540. https://doi.org/10.1091/mbc.E07-05-0480

Sacks-Zimmerman, A., Duggal, D., & Liberta, T. (2015). Cognitive Remediation Therapy for Brain Tumor Survivors with Cognitive Deficits. *Cureus*, *7*(10), e350. https://doi.org/10.7759/cureus.350

Scholzen, T., & Gerdes, J. (2000). The Ki-67 protein: from the known and the unknown. *Journal of Cellular Physiology*, *182*(3), 311–322. https://doi.org/10.1002/(SICI)1097-4652(200003)182:3<311::AID-JCP1>3.0.CO;2-9

Shmelkov, S. V., St Clair, R., Lyden, D., & Rafii, S. (2005). AC133/CD133/Prominin-1. *The International Journal of Biochemistry & Cell Biology*, *37*(4), 715–719. https://doi.org/10.1016/j.biocel.2004.08.010

Silber, J. R., Blank, A., Bobola, M. S., Ghatan, S., Kolstoe, D. D., & Berger, M. S. (1999). O6-methylguanine-DNA methyltransferase-deficient phenotype in human gliomas: frequency and time to tumor progression after alkylating agent-based chemotherapy. *Clinical Cancer Research: An Official Journal of the American Association for Cancer Research*, *5*(4), 807–814.

Singh, S. K., Clarke, I. D., Terasaki, M., Bonn, V. E., Hawkins, C., Squire, J., & Dirks, P. B. (2003). Identification of a cancer stem cell in human brain tumors. *Cancer Research*, *63*(18), 5821–5828.

Slomiany, M. G., Dai, L., Tolliver, L. B., Grass, G. D., Zeng, Y., & Toole, B. P. (2009). Inhibition of Functional Hyaluronan-CD44 Interactions in CD133-positive Primary Human Ovarian Carcinoma Cells by Small Hyaluronan Oligosaccharides. *Clinical Cancer Research*, *15*(24), 7593–7601. https://doi.org/10.1158/1078-0432.CCR-09-2317

Soroceanu, L., Gillespie, Y., Khazaeli, M. B., & Sontheimer, H. (1998). Use of chlorotoxin for targeting of primary brain tumors. *Cancer Research*, *58*(21), 4871–4879.

Soroceanu, Liliana, Manning, T. J., & Sontheimer, H. (1999). Modulation of Glioma Cell Migration and Invasion Using Cl− and K+ Ion Channel Blockers. *The Journal of Neuroscience*, *19*(14), 5942–5954.

Stern, R., Shuster, S., Neudecker, B. A., & Formby, B. (2002). Lactate stimulates fibroblast expression of hyaluronan and CD44: the Warburg effect revisited. *Experimental Cell Research*, *276*(1), 24–31. https://doi.org/10.1006/excr.2002.5508

Stockhausen, M.-T., Kristoffersen, K., & Poulsen, H. S. (2010). The functional role of Notch signaling in human gliomas. *Neuro-Oncology*, *12*(2), 199–211. https://doi.org/10.1093/neuonc/nop022

Stummer, W., Pichlmeier, U., Meinel, T., Wiestler, O. D., Zanella, F., & Reulen, H.-J. (2006). Fluorescence-guided surgery with 5-aminolevulinic acid for resection of malignant glioma: a randomised controlled multicentre phase III trial. *The Lancet Oncology*, *7*(5), 392–401. https://doi.org/10.1016/S1470-2045(06)70665-9

Stupp, R., Brada, M., Bent, M. J. van den, Tonn, J.-C., & Pentheroudakis, G. (2014). High-grade glioma: ESMO Clinical Practice Guidelines for diagnosis, treatment and follow-up. *Annals of Oncology*, *25*(suppl 3), iii93–iii101. https://doi.org/10.1093/annonc/mdu050

Stupp, Roger, Hegi, M. E., Gilbert, M. R., & Chakravarti, A. (2007). Chemoradiotherapy in Malignant Glioma: Standard of Care and Future Directions. *Journal of Clinical Oncology*, *25*(26), 4127–4136. https://doi.org/10.1200/JCO.2007.11.8554

Stupp, Roger, Hegi, M. E., Mason, W. P., van den Bent, M. J., Taphoorn, M. J. B., Janzer, R. C., … National Cancer Institute of Canada Clinical Trials Group. (2009). Effects of radiotherapy with concomitant and adjuvant temozolomide versus radiotherapy alone on survival in glioblastoma in a randomised phase III study: 5-year analysis of the EORTC-NCIC trial. *The Lancet. Oncology*, *10*(5), 459–466. https://doi.org/10.1016/S1470-2045(09)70025-7

Tang, W., Chang, S. B., & Hemler, M. E. (2004). Links between CD147 function, glycosylation, and caveolin-1. *Molecular Biology of the Cell*, *15*(9), 4043–4050. https://doi.org/10.1091/mbc.e04-05-0402

Teng, Y., Zeisberg, M., & Kalluri, R. (2007). Transcriptional regulation of epithelial-mesenchymal transition. *Journal of Clinical Investigation*, *117*(2), 304–306. https://doi.org/10.1172/JCI31200

The Cancer Genome Atlas Research Network (TCGA). (2015). Comprehensive, Integrative Genomic Analysis of Diffuse Lower-Grade Gliomas. *The New England Journal of Medicine*, *372*(26), 2481–2498. https://doi.org/10.1056/NEJMoa1402121

Ullrich, N., Gillespie, G. Y., & Sontheimer, H. (1995). Human astrocytoma cells express a unique chloride current. *Neuroreport*, *7*(1), 343–347.

van Dijk, E. L., Auger, H., Jaszczyszyn, Y., & Thermes, C. (2014). Ten years of next-generation sequencing technology. *Trends in Genetics*, *30*(9), 418–426. https://doi.org/10.1016/j.tig.2014.07.001

Vaupel, P., Mayer, A., & Höckel, M. (2004). Tumor Hypoxia and Malignant Progression. In B.-M. in Enzymology (Ed.) (Vol. 381, pp. 335–354). Academic Press. Retrieved from http://www.sciencedirect.com/science/article/pii/S0076687904810231

Veiseh, M., Gabikian, P., Bahrami, S.-B., Veiseh, O., Zhang, M., Hackman, R. C., … Olson, J. M. (2007). Tumor Paint: A Chlorotoxin:Cy5.5 Bioconjugate for Intraoperative Visualization of Cancer Foci. *Cancer Research*, *67*(14), 6882–6888. https://doi.org/10.1158/0008-5472.CAN-06-3948

Verhaak, R. G. W., Hoadley, K. A., Purdom, E., Wang, V., Qi, Y., Wilkerson, M. D., … Hayes, D. N. (2010). Integrated Genomic Analysis Identifies Clinically Relevant Subtypes of Glioblastoma Characterized by Abnormalities in PDGFRA, IDH1, EGFR, and NF1. *Cancer Cell*, *17*(1), 98–110. https://doi.org/10.1016/j.ccr.2009.12.020

Vescovi, A. L., Galli, R., & Reynolds, B. A. (2006). Brain tumour stem cells. *Nature Reviews Cancer*, *6*(6), 425–436. https://doi.org/10.1038/nrc1889

Visvader, J. E., & Lindeman, G. J. (2008). Cancer stem cells in solid tumours: accumulating evidence and unresolved questions. *Nature Reviews Cancer*, *8*(10), 755–768. https://doi.org/10.1038/nrc2499

Voigt, H., Vetter-Kauczok, C. S., Schrama, D., Hofmann, U. B., Becker, J. C., & Houben, R. (2009). CD147 Impacts Angiogenesis and Metastasis Formation. *Cancer Investigation*, *27*(3), 329–333. https://doi.org/10.1080/07357900802392675

Wang, C.-Y., Lin, C.-F., Wang, C.-Y., & Lin, C.-F. (2014). Annexin A2: Its Molecular Regulation and Cellular Expression in Cancer Development, Annexin A2: Its Molecular Regulation and Cellular Expression in Cancer Development. *Disease Markers*, *Disease Markers*, *2014*, *2014*, e308976. https://doi.org/10.1155/2014/308976, 10.1155/2014/308976

Wang, Jia, Yang, T., Xu, G., Liu, H., Ren, C., Xie, W., & Wang, M. (2016). Cyclin-Dependent Kinase 2 Promotes Tumor Proliferation and Induces Radio Resistance in Glioblastoma. *Translational Oncology*, *9*(6), 548–556. https://doi.org/10.1016/j.tranon.2016.08.007

Wang, Jialiang, Wang, H., Li, Z., Wu, Q., Lathia, J. D., McLendon, R. E., … Rich, J. N. (2008). c-Myc Is Required for Maintenance of Glioma Cancer Stem Cells. *PLoS ONE*, *3*(11). https://doi.org/10.1371/journal.pone.0003769

Wang, Jingda, & Zhang, Q. (2015). Targeting glioblastoma cancer stem cell marker CD133 by heptapeptide-modified DSPE-PEG micelles. *Journal of Chinese Pharmaceutical Sciences*, *24*. https://doi.org/10.5246/jcps.2015.01.004

Watanabe, T., Vital, A., Nobusawa, S., Kleihues, P., & Ohgaki, H. (2009). Selective acquisition of IDH1 R132C mutations in astrocytomas associated with Li-Fraumeni syndrome. *Acta Neuropathologica*, *117*(6), 653–656. https://doi.org/10.1007/s00401-009-0528-x

Waters, K. M., Stenoien, D. L., Sowa, M. B., von Neubeck, C., Chrisler, W. B., Tan, R., … Weber, T. J. (2013). Annexin A2 Modulates Radiation-Sensitive Transcriptional Programming and Cell Fate. *Radiation Research*, *179*(1), 53–61. https://doi.org/10.1667/RR3056.1

Weidle, U. H., Scheuer, W., Eggle, D., Klostermann, S., & Stockinger, H. (2010). Cancer-related issues of CD147. *Cancer Genomics & Proteomics*, *7*(3), 157–169.

Wen, P. Y., & Kesari, S. (2008). Malignant Gliomas in Adults. *New England Journal of Medicine*, *359*(5), 492–507. https://doi.org/10.1056/NEJMra0708126

Wiranowska, M., Colina, L. O., & Johnson, J. O. (2011). Clathrin-mediated entry and cellular localization of chlorotoxin in human glioma. *Cancer Cell International*, *11*, 27. https://doi.org/10.1186/1475-2867-11-27

Wojton, J., Meisen, W. H., & Kaur, B. (2015). How to train glioma cells to die: molecular challenges in cell death. *Journal of Neuro-Oncology*. https://doi.org/10.1007/s11060-015-1980-1

Wollmann, G., Ozduman, K., & van den Pol, A. N. (2012). Oncolytic Virus Therapy of Glioblastoma Multiforme – Concepts and Candidates. *Cancer Journal (Sudbury, Mass.)*, *18*(1), 69–81. https://doi.org/10.1097/PPO.0b013e31824671c9

Xu, T., Fan, Z., Li, W., Dietel, B., Wu, Y., Beckmann, M. W., … Savaskan, N. E. (2016). Identification of two novel Chlorotoxin derivatives CA4 and CTX-23 with chemotherapeutic and anti-angiogenic potential. *Scientific Reports*, *6*, 19799. https://doi.org/10.1038/srep19799

Xu, X., Zhao, J., Xu, Z., Peng, B., Huang, Q., Arnold, E., & Ding, J. (2004). Structures of Human Cytosolic NADP-dependent Isocitrate Dehydrogenase Reveal a Novel Self-regulatory Mechanism of Activity. *Journal of Biological Chemistry*, *279*(32), 33946–33957. https://doi.org/10.1074/jbc.M404298200

Yan, H., Bigner, D. D., Velculescu, V., & Parsons, D. W. (2009). Mutant Metabolic Enzymes Are at the Origin of Gliomas. *Cancer Research*, *69*(24), 9157–9159. https://doi.org/10.1158/0008-5472.CAN-09-2650

Yan, Hai, Parsons, D. W., Jin, G., McLendon, R., Rasheed, B. A., Yuan, W., … Bigner, D. D. (2009). *IDH1* and *IDH2* Mutations in Gliomas. *New England Journal of Medicine*, *360*(8), 765–773. https://doi.org/10.1056/NEJMoa0808710

Yang, Z., Zhang, L., Zhang, Y., Zhang, T., Feng, Y., Lu, X., … Wang, X. (2011). Highly Efficient Production of Soluble Proteins from Insoluble Inclusion Bodies by a Two-Step-Denaturing and Refolding Method. *PLoS ONE*, *6*(7), e22981. https://doi.org/10.1371/journal.pone.0022981

Yoshida, S., Shibata, M., Yamamoto, S., Hagihara, M., Asai, N., Takahashi, M., … Kadomatsu, K. (2000). Homo-oligomer formation by basigin, an immunoglobulin superfamily member, via its N-terminal immunoglobulin domain. *European Journal of Biochemistry*, *267*(14), 4372–4380.

Yu, R., Wang, J., Li, J., Wang, Y., Zhang, H., Chen, J., … Liu, X. (2010). A novel cyclopeptide from the cyclization of PACAP(1–5) with potent activity towards PAC1 attenuates STZ-induced diabetes. *Peptides*, *31*(6), 1062–1067. https://doi.org/10.1016/j.peptides.2010.03.008

Zhai, H., Acharya, S., Gravanis, I., Mehmood, S., Seidman, R. J., Shroyer, K. R., … Tsirka, S. E. (2011). Annexin A2 promotes glioma cell invasion and tumor progression. *The Journal of Neuroscience: The Official Journal of the Society for Neuroscience*, *31*(40), 14346–14360. https://doi.org/10.1523/JNEUROSCI.3299-11.2011

Zhang, J., Stevens, M. F. G., & Bradshaw, T. D. (2012). Temozolomide: mechanisms of action, repair and resistance. *Current Molecular Pharmacology*, *5*(1), 102–114.

Zhang, W., Caskey, L. S., Fuller, G. N., Bruner, J. M., Yung, W. K. A., Sawaya, R. E., & Holland, E. C. (2000). Toward a molecular classification of the gliomas: histopathology, molecular genetics, and gene expression profiling. *Histology and Histopathology*, *15*(3), 971–981.

Zhang, Z., Huang, L., Zhao, W., & Rigas, B. (2010). Annexin 1 induced by anti-inflammatory drugs binds to NF-kappaB and inhibits its activation: anticancer effects in vitro and in vivo. *Cancer Research*, *70*(6), 2379–2388. https://doi.org/10.1158/0008-5472.CAN-09-4204

Zhao, P., Zhang, W., Wang, S.-J., Yu, X.-L., Tang, J., Huang, W., … Chen, Z.-N. (2011). HAb18G/CD147 promotes cell motility by regulating annexin II-activated RhoA and Rac1 signaling pathways in hepatocellular carcinoma cells. *Hepatology*, *54*(6), 2012–2024. https://doi.org/10.1002/hep.24592

Zhao, S., Lin, Y., Xu, W., Jiang, W., Zha, Z., Wang, P., … Xiong, Y. (2009). Glioma-Derived Mutations in IDH1 Dominantly Inhibit IDH1 Catalytic Activity and Induce HIF-1. *Science*, *324*(5924), 261–265. https://doi.org/10.1126/science.1170944

Zheng, H., Ying, H., Yan, H., Kimmelman, A. C., Hiller, D. J., Chen, A.-J., … DePinho, R. A. (2008). Pten and p53 Converge on c-Myc to Control Differentiation, Self-renewal, and Transformation of Normal and Neoplastic Stem Cells in Glioblastoma. *Cold Spring Harbor Symposia on Quantitative Biology*, *73*, 427–437. https://doi.org/10.1101/sqb.2008.73.047

Zhu, T. S., Costello, M. A., Talsma, C. E., Flack, C. G., Crowley, J. G., Hamm, L. L., … Fan, X. (2011). Endothelial Cells Create a Stem Cell Niche in Glioblastoma by Providing NOTCH Ligands That Nurture Self-Renewal of Cancer Stem-Like Cells. *Cancer Research*, *71*(18), 6061–6072. https://doi.org/10.1158/0008-5472.CAN-10-4269

Zoltan-Jones, A., Huang, L., Ghatak, S., & Toole, B. P. (2003). Elevated hyaluronan production induces mesenchymal and transformed properties in epithelial cells. *The Journal of Biological Chemistry*, *278*(46), 45801–45810. https://doi.org/10.1074/jbc.M308168200

Zucker, S., Hymowitz, M., Rollo, E. E., Mann, R., Conner, C. E., Cao, J., … Toole, B. P. (2001). Tumorigenic potential of extracellular matrix metalloproteinase inducer. *The American Journal of Pathology*, *158*(6), 1921–1928. https://doi.org/10.1016/S0002-9440(10)64660-3